Physico-Chemical Properties of Tristearin-Oil Blends

By

Huixin Du

A thesis submitted to the

Graduate School-New Brunswick

Rutgers, The State University of New Jersey

In partial fulfillment of the requirements

For the degree of

Master of Science

Graduate Program in Food Science

Written under the direction of

Dr. Michael A. Rogers

And approved by

_____

_____

_____

New Brunswick, New Jersey

October 2015

ABSTRACT OF THE THESIS

Physico-Chemical Properties of Tristearin-Oil Blends

By HUIXIN DU

Thesis Director:

Michael A. Rogers

In order to understand how the chemical structure of liquid oil influences the crystallization process of hardstock fats, a set of binary triglycerides systems were made of either tristearin with one medium chain triglycerides (MCT) or tristearin with one unsaturated triglyceride. The system is assessed in terms of microstructure, kinetics, and phase behavior using differential scanning calorimetry (DSC), polarized light microscopy (PLM), small deformation rheology and nuclear magnetic resonance (pNMR). For unsaturated triglycerides, irrespective of the dilution factor used, the mode of nucleation remained instantaneous, while for medium chain triglycerides the mode of nucleation changed from instantaneous to sporadic when the samples were diluted beyond 70% oil. The fractal dimension results also indicated that MCTs altered the crystal microstructure of tristearin differently than unsaturated triglycerides. The solubility curve further confirmed that the unsaturated oil blends obeyed ideal solubility while MCTs oils probably co-crystalized with tristearin and

did not act as a simple dilution factor. The work from this thesis provide theoretical evidence that it is possible to manipulate the structure and thus the properties of hardstock fat by incorporating different types of oils.

On the other hand, the confinement effect of the solid fat also alters the micro-viscosity of the liquid oils embedded in the oil-fat blends. The micro-viscosity of the liquid oil in the system was measured by fluorescence spectroscopy using Citrus red (CR) 2 as a luminescent molecular rotor. The viscosity decreases as the solid content of tristearin decrease but the trends did not show strong correlations. On the other hand, a strong log-logistic correlation between box-counting fractal dimension and normalized intensity of CR is observed in high-space filling colloidal fat crystal networks. Based on these results, we suggest that the use of bulk oil viscosity to predict diffusion/oil migration in multi oil phase may not be appropriate.

ACKNOWLEDGEMENTS

The three year pursuit of my Master's degree at Rutgers was such a memorable shinning piece in my life, fulfilled with the growth of not only academic knowledge but also courage to deal with challenges in life. I never imagine going abroad alone and studying in a foreign langue to be an easy road, still it was even harder than what I anticipated. It is tough to struggle in those frustrated, helpless and even desperate moments and face the weakness of myself, but passing through that darkness make me a stronger person and helped me figure out what I really want to be and finally get back the confidence and passion. Now I can say I am really proud of what I have achieved today and looking back I am so grateful to the people who gave me support, company, guidance and suggestions along this journey.

I could've never got this far without the support of my parents, Qiulian and Zhifeng. Although they are not in US with me, no matter what happens I can always count on them for help, support and comfort. When I am about to give up or avoid the difficulties in study or research family is always the place where I find courage to defeat my weakness. Their wisdom can always help me find the best solution to solve the problem and their unconditional support and back up kept me strong and positive. Their love is so selfless and powerful and I could never appreciate more for their love.

Dr. Michael A. Rogers, my advisor throughout my Masters career at Rutgers University, has been a great mentor. His guidance was crucial to ensure that I always worked in the right direction and he let me know what I needed to improve in order to

be a qualified scientist, not just for the degree. He is always patient with our questions, dedicate to instruct me on my thesis and encourage me to keep improving myself. He is respectful to our choices and supports me as a friend. I feel so honored to have the chance to learn from him and work with him.

I would also like to express my gratitude to Dr. Corradini, who instructed me on fluorescence spectroscopy, the results of that study are included in section 5 of this thesis. Her enthusiasm towards science infected me and made me realize that science is the process to solve problems and there are always more solutions than problems as long as you are determined enough. I will carry on her spirit with me in the future when meeting greater challenges. I would also like to thank my defense committee members, Dr. Ludescher, Dr. Rogers and Dr. Corradini, for their discussion and comments.

Last but no least I want to thank all of my friends who accompanied me and enlightened me with their knowledge and ideas, especially all my lab mates who helped me during my work and thesis; and roommates who share all the happiness and sadness during my studies in US.

And in the end I want to say life is full of challenge and chance and I can't wait to meet them. I will keep working hard, thinking positively, trying to be a qualified and passionate scientist.

PREFACE

The research presented in this thesis was conducted in the Department of Food Science, School of Environmental and Biological Sciences, Rutgers, The State University of New Jersey. It is a result of my work during the period between September 2012 and May 2014.

Chapter five (5) of is co-authored by Dr. Michael A. Rogers, Christina Kim, Maria G. Corradini and Richard D. Ludescher RD. With pride, this chapter has been published in *Soft Matter:* the article is entitled "Micro-viscosity of liquid oil confined in colloidal fat crystal networks", (DOI:10.1007/s00396-014-3480-9) , Published: Dec, 2014.

Table of Contents

1 Introduction

The excessive consumption of saturated and *trans* fats has long been proved to positively correlate to coronary heart disease by changing the cholesterol composition, mainly the ratio of low-density lipoprotein (LDL) to high-density lipoprotein (HDL)[1, 2]. People's craving for high fat products including cream, butter, margarine and chocolate is hard to give up since fats provides a wide variety of oral sensation such as thickness, smoothness and creaminess[3]. The main contribution of the satisfactory sensation comes from the hardstock fats, the solid continuous networks of fat crystals composed of various saturated and *trans* fats, which determines the textural and organoleptic properties in high fat food products[4]. Therefore the basic understanding of the fat crystal networks is critical if we want to manipulate it and make it healthier without sacrificing the sensory properties.

In high fat content food products (with a lipid continuous phase), the solid fat network is not there alone and there is always liquid oil trapped inside the crystalline network and the ratio as well as the interactions between the solid and liquid components play important roles in determining the final texture. Therefore the solvent effect of liquid oils on solid fat is studied. Wright et al. studied the crystallization behavior of high melting fractions of milk fat (HMF) in canola oil and low-melting fraction of milk fat (LMF) and found more solids were formed in LMF than canola oils possibly because of molecular complementarity[5]. Zhou and Hartel also studied the solubility of some high-melting temperature fats (e.g., cocoa butter,

palm) in low-melting temperature oils (e.g., canola oil, sunflower oil)[6]. However, most of the studies related to this topic use fats and oils that are composed of a combination of a variety of triglycerides instead of the single triglyceride. Thus it is hard to conclude which triglycerides or what aspect of the triglycerides are responsible for differences in the solids properties. One of the goals of this thesis is to build a simplified system with pure triglycerides and try to understand how the structural differences of the oil triglycerides affect the crystallization of the solid triglycerides.

On the other hand, the effect of constraints imposed by the solid fat networks on liquid oils are also of great importance in confectionary fats with respect to oil migration in products such as chocolates and cream fillings which may shorten the shelf life[7]. The hardness and the mouthfeel can change dramatically with time when oil migration occurs. The oil migration mechanism is not well understood yet. One of the preferred explanations is oil diffusion, which occurs because of the concentration gradients of triglycerides, and the oil diffusivity is closely related to viscosity of the liquid triglycerides [7, 8]. So the second goal of this thesis is to find out how the fat crystal networks affect the micro viscosity of the liquid oils trapped in the system. Traditional viscosity measurements include capillary viscometer, falling ball viscometer and rotary viscometer all of which measure the internal friction of the system representing a measure of the macro viscosity[9]. When it comes to the viscosity of a particular local area, sensors and optical methods such as fluorescence anisotropy and fluorescence recovery after photo bleaching[10, 11] are better suited to

characterize the system. Molecular rotors acting as local viscosity probes have been employed to study biological materials in recent decades. The work in this thesis also explored the possibility of using GRAS food additives as micro viscosity probes in semisolid matrices in order to offer a non-disruptive and highly sensitive alternative to conventional measurements of bulk and local viscosity.

2 Literature Review

2.1 Lipids

2.1.1 Fatty acids and triglycerides

Lipids are a group of compounds that are soluble in organic solvents. They are most broadly subdivided into “fats” and “oils” where fats refer to lipids that are solid at ambient temperature and oils are liquid. The major components of lipids are fatty acids that are comprised of a straight aliphatic chain, of varying length and degrees of saturation and a carboxylic acid group. The majority of fatty acids have carbon numbers between 14 and 24 and most natural fatty acids have an even number of carbons since two carbons are always added at a time during biological elongation[12]. According to the number of carbons in the aliphatic chain, fatty acids can be sub-classified as short/medium/long chain fatty acids[13, 14]. According to the saturation and the type of saturation of aliphatic chain, there are saturated fatty acids (with no double bond), *cis* unsaturated fatty acids (with one or more *cis* double bonds) and *trans* unsaturated fatty acids (with one or more *trans* double bonds). Fatty acids with an odd carbon number and branched chains are rare in nature especially in plants, but they can be found in milk and adipose tissue of ruminant animals such as cattle and sheep and also in microorganisms[15-18]. The fatty acid composition of the foods varies with the source. Generally most vegetable oils are highly unsaturated and the amount of saturated fatty acids, mainly palmitic and stearic, from animal source are in the order of milk > sheep > beef > pig > chicken >turkey > marine[12].

Over 99% of the fatty acids found in foods are esterified to glycerol, existing as mono-, di-, tri esters called monoglycerides, diglycerides and triglycerides among which triglycerides are the most common form[12]. Triglycerides are composed of one glycerol molecule esterified to three fatty acids, that may either be the same or different (Figure 1). For plants triglycerides, typically the unsaturated fatty acids are located at position 2 and saturated fatty acids are located at position 1 and 3, while for animal triglycerides, fatty acids distribution differs among species and the location of animal and generally there are more saturated fatty acids attached at position 2[19, 20]. Generally, the *-ic* at the end of the fatty acid will be replaced with *–oyl* and *sn*-1, -2, -3 is used to describe the fatty acid location on the glycerol. For example if a triglyceride contains stearic acid, palmitic acid and oleic acid at positions 1, 2 and 3, the name will be 1-stearoyl-2-palmitoly-3-oleoyl-sn-glycerol. Both the type of the fatty acids in triglycerides and the positional distribution affect the physical properties of triglycerides such as melting point and crystal polymorphism that, in turn, affect the mechanical properties of natural fats[21]. Generally, the higher number of double bonds in fatty acids which forms the triglycerides, the lower melting point of the triglycerides. Segura et al. studied the fatty acids positional distribution within triglycerides in dry-cured ham subcutaneous fat and found that hardness is positively correlated with C16, C18 at the *sn*-1, 3 and adhesiveness is related to fatty acids in the *sn*-2 position and inversely correlates with mono-unsaturated fatty acid and unsaturation index[22].

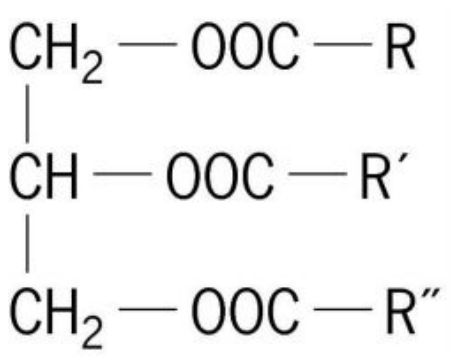

Figure 1. Chemical structure of triglycerides composed of a glycerol backbone and three fatty acids esterified on Sn1-, Sn2- and Sn3- positions.

2.1.2 Health concerns related to the excessive intake of fats

In the past few decades, national dietary recommendations mainly focused on emphasizing the reduction in total fat intake in order to lower the risk of coronary heart disease (CHD)[23]. However recent evidence demonstrated that the type of fat rather than total amount of fat better predict serum cholesterol levels that are linked to the risk of CHD[23]. A study investigated the intake of individual fatty acids in relation to mortality rate from CHD, and the results showed a strong positive correlation between rates from CHD and intake of saturated and *trans* fatty acids[2]. The ratio of total to high density lipoprotein (HDL) cholesterol can be used as a factor to evaluate the risk of CHD since high concentrations of HDL cholesterol are proven to help to prevent CHD diseases[24-26]. The study from Patty et al. showed that the total:HDL ratio did not change when saturated fatty acids were replaced by carbohydrates but the ratio decreased when saturated fatty acids or *trans* fatty acids were substituted by cis unsaturated fatty acids [27].The 2010 Dietary Guideline for Americans recommends limiting the amount of saturated fatty acids to be lower than

10% of the calorie intake by replacing them with monounsaturated and polyunsaturated fatty acid, and consuming as little *trans* fat as possible and reducing solid fat intake[28].

2.1.3 Health benefits of unsaturated fatty acids

The concentration of LDL is directly related to the CHD incidence while HDL concentration is inversely associated with development of CHD and they are regarded as effective predictors for coronary heart disease as well as evaluating the risk of the CHD[29-33]. The meta-analysis for 27 trials by Mensink showed that substituting saturated fatty acid with unsaturated fatty acid led to a higher ratio of HDL to LDL cholesterol and gave more favorable serum lipid profiles in regards to lowering the risk of CHD[27]. Similar effects were also found by Mattson, where oleic acid and linoleic acid help reduce the LDL-C level in the plasma among male patients[34]. Dietary and supplemental intake of n-3 polyunsaturated fatty acids could reduce mortality caused by myocardial infarction, and sudden death among CHD patients [35]. According to the 2010 Dietary Guidelines for Americans, the consumption of the saturated fat is too high while the mono and polyunsaturated fatty acid is insufficient which leads to the recommendation to replace some animal fats such as butter and lard with vegetable oils rich in unsaturated fatty acid[28]. Also The American Heart Association recommends that less than 5% to 6% of calories should come from saturated fats which correspond to no more than 13g saturated fats (calculated based on 2000 daily calories consumption).

2.1.4 Health benefits of medium chain triglycerides (MCTs)

Triglycerides containing fatty acids with a chain length from 6 to 12 carbon atoms are usually called medium chain triglycerides and those with chain length more than 14 are called long chain triglycerides[36]. The metabolic pathway of medium chain triglycerides in the human body is different from that of long chain triglycerides. They are rapidly hydrolyzed to medium chain fatty acids and then directly delivered to the liver where they can be oxidized to ketones. They do not go through the process of re-synthesis of triglycerides in intestinal cells[37]. The differences of the absorption channel from long chain triglycerides give them ability to serve as an energy source for patients suffering from fat malabsorption and pancreatic insufficiency since 1950s[38].

Recently studies showed that compared to long chain triglycerides (LCTs), diets rich in medium chain triglycerides (MCTs) have certain benefits especially with respect to body weight. A weight loss diet study among 48 overweight men and women showed that the consumption of MCTs oils ends up in more weight and fat mass loss compared with olive oils and suggested that MCTs oils can be included into weight-loss diet[39]. Similar studies also showed that MCTs diets could reduce body weight and suppress accumulation of body fat in healthy individuals more than LCTs [40, 41], partially by increasing the energy expenditure and generating greater satiety[42, 43]. Therefore MCTs may play a role in body weight control and obesity

treatment.

2.2 Fat crystallization

Crystallization of fats is a phase transition process where triglycerides molecules go from an amorphous liquid state to an ordered solid state. Natural fats/oils are complex mixtures of hundreds of triglycerides with various melting points and other physical properties, which result in complex crystallization profiles at different temperatures. The resulting three-dimensional network of fat crystals provides the solid structure, or the "plasticity" of fats which is a crucial character of most fat-containing products such as butter, chocolate, shortening and spreads. The crystallization properties include crystal morphology, polymorphic form and solid fat content and these parameters determine the final mechanical and sensory characteristics of the product[12]. Crystallization can be generally discussed as two processes, the nucleation process followed by crystal growth.

2.2.1 Nucleation

2.2.1.1 Nucleation mechanism

The physical state of a triglyceride mixture, at a specific temperature, is determined by the Gibbs free energy of the system[12]. When the temperature of a triglyceride melt drops below its melting point, the solid state is favored. However, the formation of a new phase (nucleus) will not occur right after the temperature

crosses the melting point boundary, instead a metastable state persists and triglycerides remain in a liquid state below its melting point; this state is referred to as a supercooled or undercooled metastable state, which is due to the opposing activation energy that needs to be overcome before the formation of nuclei[44-46]. For fats, initiation of solidification usually requires 5 to 10 degrees of undercooling below the melting point[45]. Upon nucleation, triglycerides molecules tend to interact via Van der Waal's forces, creating tiny nuclei embryos. During this process, the chemical potential of the system is lowered. Meanwhile, the creation of the new interface associated with the new nuclei serves as an opposing thermodynamic driving force preventing the formation of nuclei[45]. As a result, the crystal embryos may not be stable and may form and break continuously until the nucleus reaches a critical size, where the gain of the free energy by creation a new interface is less than the loss of the free energy by lowering the chemical potential. The Gibbs free energy change of nucleus formation can be expressed as[45]:

$$\Delta G = A\gamma - V\frac{\Delta\mu}{V_{ms}} \quad (1)$$

where A is the surface area of the a nucleus, γ is the crystal melt interfacial tension (J m^{-2}) associated with the new surface, V is the volume of the nucleus (m^3), $\Delta\mu$ is the difference of chemical potential (J mol^{-1}) between the solid and liquid state and V_{ms} is the solid molar volume ($m^3\,mol^{-1}$). The formula demonstrates a volume term that favors nucleation and a surface term that impedes nucleation. If the nucleus is spherical with a radius of r (m) then the free energy can be written as[45]

$$\Delta G = 4\pi r^2\gamma - \frac{4}{3}\pi r^3 \frac{\Delta\mu}{V_{ms}}, \quad (2)$$

and the change of the ΔG with radius is shown in Figure 2.

The newly formed nuclei will be stable and continue to grow into stable crystals as long as the radius of the nuclei is larger than the critical radius, r_c, defined in Eq. 3, otherwise the nuclei will dissolve.

$$r_c = \frac{2\Upsilon T_m}{\Delta H_f \Delta T} \quad (3)$$

where ΔH_f is the enthalpy change per unit volume of fusion, T_m is the melting point, ΔT is the degree of super cooling. The critical size, r_c, required to form stable nuclei decreases with an increasing degree of supercooling ΔT, as well the nucleation rate will also increase.

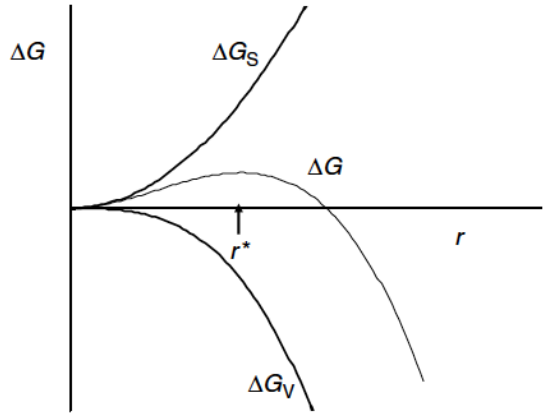

Figure 2. Free energy change for different nuclei size. The free energy change is determined by the combination of a negative volume term (ΔG_v) and a positive free energy change (ΔG_s) and the critical size of nucleus corresponds to the maximum value of ΔG. Taken from reference [12].

2.2.1.2 Nucleation kinetics

The nucleation rate changes as a function of the degree of undercooling and goes

from near zero at low cooling rate to almost instantaneous at high cooling rates[47]. The relationship between nucleation rate (J) and degree of supercooling (ΔT) is illustrated in Figure 3. Under sufficiently high supercooling conditions the nucleation rate jumps from near zero to very high value and instantaneous nucleation is observed.

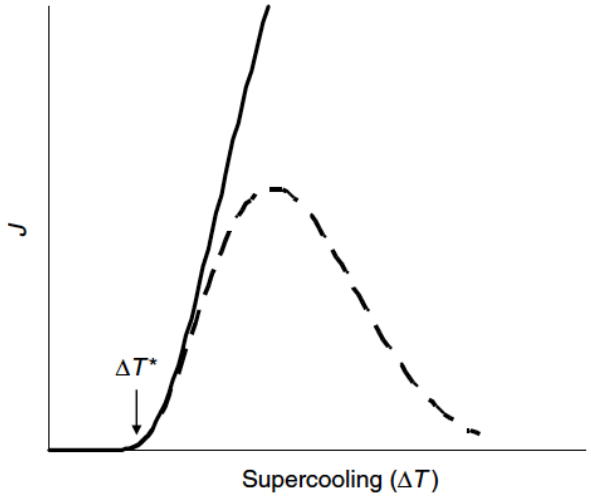

Figure 3. Relationship between nucleation rate and degree of supercooling. Solid line is the theoretically trend and dash line is practical trend. Nucleation drops after the degree of supercooling increases to a certain value due to the resulting high viscosity that hinders the diffusion of the triglyceride molecules. Taken from reference [12].

The induction time, which is the time needed for the formation of nuclei under certain supercooling conditions, is used to describe the cooling rate and is considered to be inversely proportional to nucleation rate. It can be determined experimentally by pNMR, turbidimetry, differential scanning calorimetry, polarized light microscopy and light scattering techniques[48]. The challenge for induction time measurements is

the low sensitivity of the initial nuclei event and the fact that nucleation and crystal growth are not exclusive and it is hard to distinguish them[45].

2.2.2 Crystal growth

Formation of a stable nucleus is followed by crystal growth, which is a mass and heat transfer process including a) triglyceride molecules diffusing from the liquid phase to the interface between the existing nucleus/crystals and the melt; b) molecules at the interface are incorporated into the crystal lattice in a certain manner; and, c) latent heat from the interface is removed during the mass transfer[49]. Any environmental condition that affects mass or heat transfer such as viscosity, temperature profile and mechanical agitation will have an influence on the rate of crystal growth[12]. The crystal growth mechanism depends on both internal properties of the molecules (e.g., molecular structure) and the crystallization condition (e.g., cooling rate) and thus could develop into different polymorphic type as well as different crystal shapes such as spherulitic, plate-like and feather-like[50].

The nucleation process may not stop after the start of crystal growth. Instead, they always accompany each other during supercooling but with different rates. If the nucleation rate is higher than the crystal growth rate, then small crystals tend to persist, while if the crystal growth rate is high, the crystal growth process is favored and will lead to fewer crystals but with large sizes[12]. The relative value of the nucleation rate and growth rate under different degrees of supercooling is shown in

Figure 4. One study showed that milk fat, under rapid cooling, tends to develop numerous, small crystals and smaller amount of larger crystals under slow cooling rates[51]. It is important to control supercooling in the food industry to achieve a desired crystal size in the product. This is because often sensory properties are linked to crystal size since larger crystals can be detected which means the loss of creamy and smooth mouth feel [49]

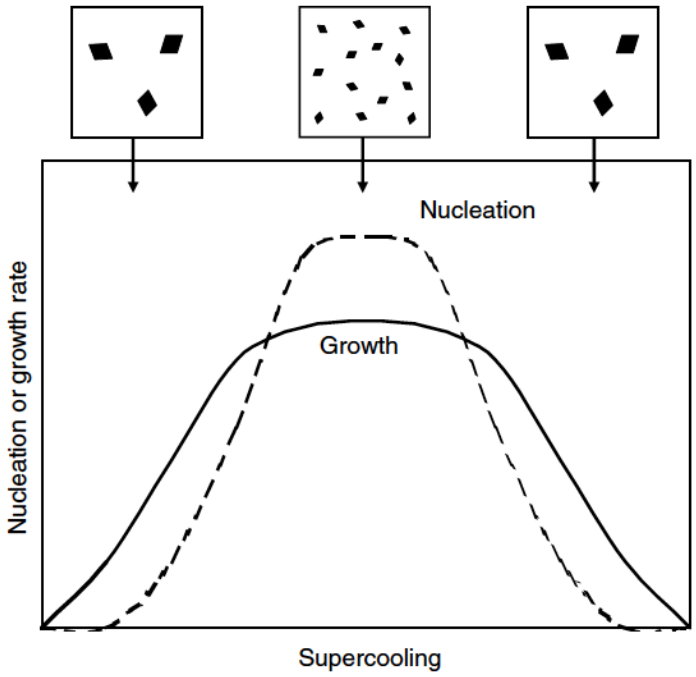

Figure 4. Growth and nucleation rates at various degrees of supercooling. The nucleation and crystal growth rates share similar trends. The relative value of the nucleation and crystal growth rates determines the crystal size and different supercooling conditions. Taken from reference [12].

2.2.3 Characterizing the liquid-solid phase transition using the Avrami model

2.2.3.1 History of development

The Avrami model was first developed to characterize the liquid-solid phase

transition in metals. In the 1940s, Avrami[52-54] gave a series of mathematical descriptions of nucleation and crystal growth process based on several statements including: a) a tiny germ nuclei primarily existing in the liquid phase and during supercooling the number of these nuclei decrease by either developing into crystals or being swallowed by the new phase; b) growth of the nuclei will cease when impingement happens between two adjacent particles; and c) the clusters of molecules can only grow when it reaches the critical size due to the associated opposing free energy change. The theory was then extended to the application of polymer crystallization in 1954[55] and later became one of the most commonly used model to study fat crystallization[56]. The model assumes isothermal crystallization conditions, randomly distributed nucleation and a linear crystal growth at all directions, which only depends on temperature but not on time[45].

2.2.3.2 Introduction of the Avrami model

The expression of the Avrami model can be slightly different depending on different derivation approaches[57]. One study adopted the derivation by Marangoni [45] and the Avrami equation for isothermal crystallization has the following form:

$$\frac{\mathrm{Y}}{\mathrm{Y_{max}}} = 1 - \mathrm{e}^{-\mathrm{kt}^{\mathrm{n}}} \qquad (4)$$

where Y is the solid volume at time t and Y_{max} is the maximum volume of the solid phase at the end of crystallization, k is the rate constant and n is the Avrami

exponent. For non-isothermal crystallization the induction time is taken into consideration:

$$\frac{Y}{Y_{max}} = 1 - e^{-k(t-Z)^n} \quad (5)$$

where Z is the induction time.

The Avrami model describes both the nucleation and the crystal growth processes during crystallization. The nucleation mode can be either instantaneous which means the nucleis appear all at once or sporadic which means the nuclei form as a function of time. As for crystal growth, there are three types including one dimentional (rod-like), two dimentional (plate-like) or three dimentional (spherulitic)[45]. Each of the two nucleation types can combine with one of the three possible crystal growth modes and the sum of the nucleation number and crystal growth number is avrami exponent (n) [45](Table 1). Therefore, by fitting the experimental data of crystallization of fats (e.g. DSC, FT-IR, PLM) with the Avrami model, n and k values may be obtained and it is possible to get an idea of the crystallization kinetics in terms of nucleation type and crystal growth mode and crystallization rate [58].

Table 1. Values of Avrami exponent, n, and the expression of the rate constant k for different nucleation and crystal growth modes. Adapted from reference [45].

Crystal growth mode	Nucleation mode	n	k
Spherical	Sporadic	4	$\pi k_g j g^2$
	Instantaneous	3	$\frac{4}{3}\pi k_g \rho_c g^2$

Plate-like	Sporadic	3	$\frac{4}{3}hk_g jg$
	Instantaneous	2	$2hk_g\rho_c$g
Rod-like	Sporadic	2	$\pi r^2 k_g j$
	Instantaneous	1	$2\pi r^2 k_g \rho_c$

In Table 2 h is crystal height (m), j is rate constant of nucleation ($m^{-3}\ s^{-1}$), g is growth rate constant for the crystal's characteristic length (s^{-1}), ρ_c is the number of crystal per unit volume (m^{-3}), k_g is rate constant of crystal growth ($m\ s^{-1}$)

2.3 Fat crystal structure

2.3.1 Hierarchies of fat crystal structures

Different levels of structures are present in fat crystal networks. For a typical crystallization process, the triglyceride molecules are first involved in nucleation from the supercooled melt, forming nuclei that grow into crystallites which further intertwine and pack closely to become primary crystals (also called microstructural elements)[4, 59]. These primary crystals then aggregate and develop into intermediate (tens of microns) and large clusters (hundreds of microns) at the microstructure level (0.25~200μm)[4]. Finally the microstructures continue to cross-link and form the final 3-D fat crystal network (Figure 5 and Figure 6).

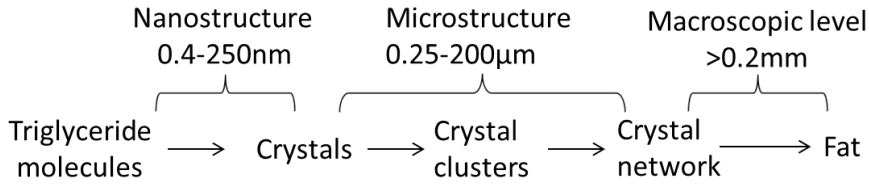

Figure 5. Different levels of structure in fat crystal networks. Adapted from reference [4].

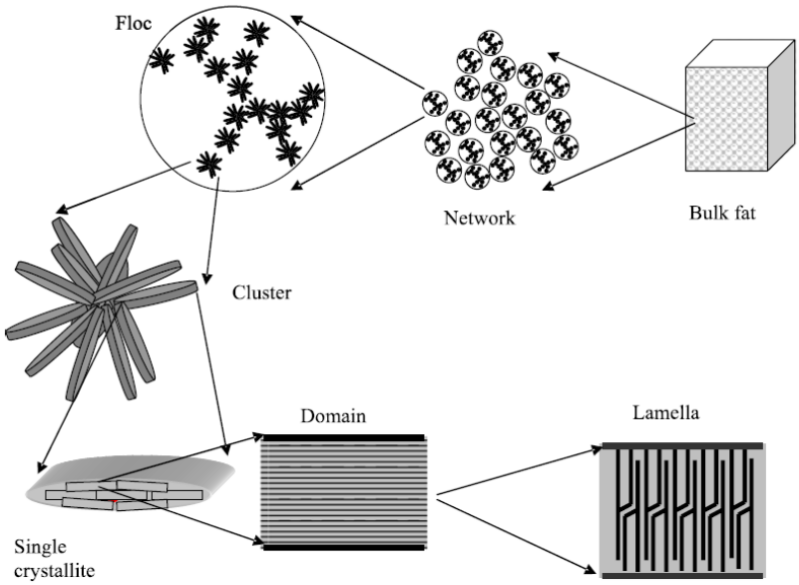

Figure 6. Schematic diagram for the formation of fat crystal networks. Taken from reference [60].

The importance of the fat crystal network structure is that it determines the viscoelastic properties and the mechanical behavior of solid fats. Their structural parameters often follow scaling relationships as a function of the solid fat content (SFC) and aid in understanding the physical properties of solid fats. Numerous properties, such as, polymorphism representing structure at the nano level has a tremendous effect on melting properties, hardness and bloom of cocoa butter in chocolates[61-64]. The SFC also closely relates to the hardness, spreadability and shortening functionality of fats [65-68]. The study at the microstructural level is not emphasized until it is found in some cases that the traditional parameters cannot give a good explanation for the physical properties difference in solid fats. Rousseau and

Hill [69-71] found that the chemical interestierified and noninteresterified milk fat have equivalent SFCs, hardness index and similar polymorph packing but differ in their shear storage moduli and microstructures which suggests that besides SFC, hardness index and polymorphism, there are other parameters that may be related to the mechanical strength of the system. The microstructure (or clusters) is the largest repeating unit in the crystal network and thus the most closely related to the macrostructure. One of the most important properties of fat crystal clusters is the inherent self-similarity[4] which is scaled by the fractal dimension, one of the parameters use to describe microstructure.

2.3.2 Fractal Analysis

2.3.2.1 Fractal nature and self-similarity

Fractal geometry was first introduced by Hausdorff[72] and then further developed by Benoit Mandelbrot[73] to describe irregular and fragmented shapes in nature such as coastlines, trees and mountains. The fractal character of natural patterns is based on their self-similar properties which describe a kind of symmetric feature - invariant against the change of the observation scale[4]. For example, if you take a small branch out of its ‘mother’ branches, take a picture of it, magnify to the size of its mother branch, the pattern of the small branch should be the same as its mother branch, at least statically. In 1983, Witten and Sander[74] studied the diffusion-limited aggregation (DLA) and found out scale-invariant features for aggregates such as dust, dentrites and other random objects. A fractal pattern was then

confirmed to exist in growing clusters by studying DLA models[75]. And the fractal dimension, which is used to quantify the fractal packing pattern is calculated for different models[76]. Later, studies on colloidal materials such as gold colloids[77] and silica aerogels[78], also confirmed scale-invariant features and the calculated fractal dimensions were in agreement with the computer simulation of diffusion-limited aggregation, indicating that fractal concept can not only describe irregular natural pattern but also disordered distributions of mass. Figure 7 shows polarized light images of high melting fraction of milk fat under different magnification which yields same fractal dimensions (D=1.60), indicating the scale-invariance of the fat crystal networks[79].

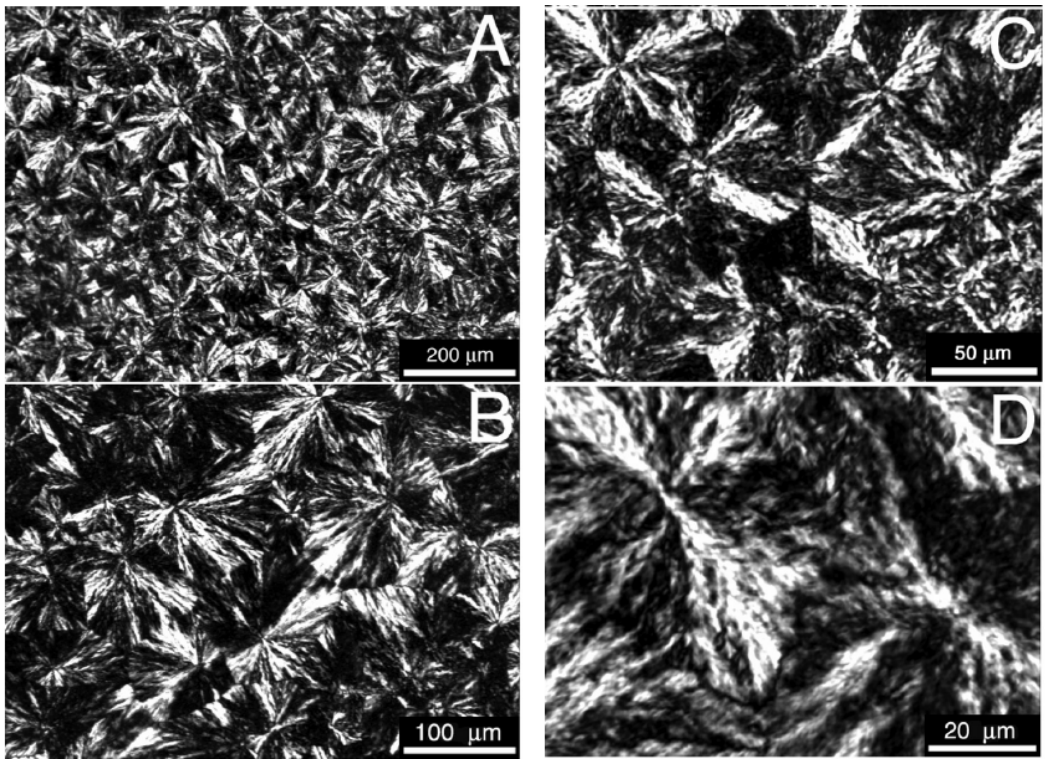

Figure 7. Polarized light micrographs of the high melting fraction of milk fat under different magnifications. The micrographs share a similar pattern under various

magnifications which indicates a self-similar property. Taken from reference [79].

2.3.2.2 Fractal dimensions

2.3.2.2.1 General concept

In traditional Euclidian geometry, the objects described are always regular including: a line (one-dimensional), a plane (two-dimensional) or a cube (three-dimensional). Compared to the fractal object mentioned above, Euclidian scale has limitations and thus the fractal dimension was developed. For example, a coastline can be seen as a curve with kinks that is neither a line nor a plane and thus will have a fractal value between one and two. Fat crystal networks share a same pattern as a flocculated colloid[80, 81] where a fractal pattern demonstrating self-similarity within the micrometer range. Figure 8 shows a simplified picture explaining aggregated particles compared to Euclidian dimensions[4]. The fractal feature is only found within certain range of the scales, below or above are all considered as homogeneous and for fat, the fractal nature can be observed within microstructure scale that is crystal clusters. The two commonly used methods to measure fractal dimension are small deformation dynamic rheological experiments and polarized microscopy image analysis.

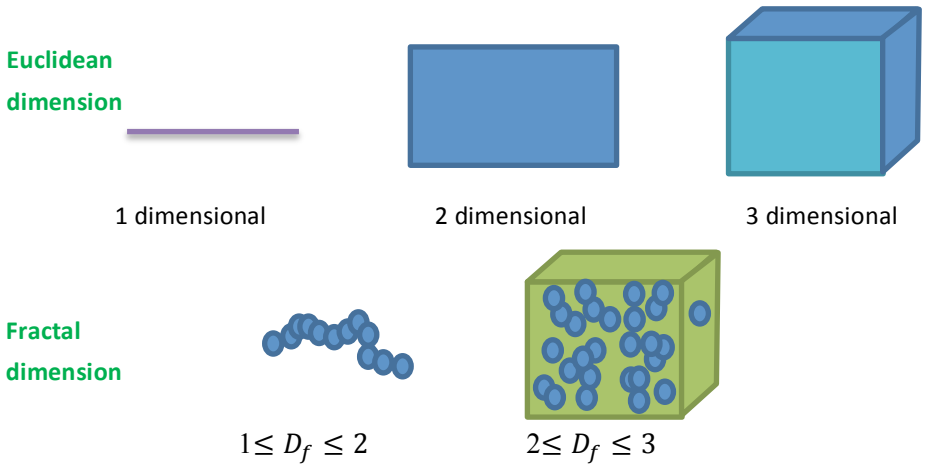

Figure 8. Schematic representation of Euclidean and Fractal dimensions. Adapted from reference [4].

2.3.2.2.2 Fractal dimensions determined by microscopy methods

Numerous microscopic methods can be used to observe fat crystals such as scanning electron microscopy (SEM), polarized microscopy (PLM), confocal laser scanning microscopy and atomic force microscopy (AFM). Among them, freeze-fracture SEM is good to visualize the surface structure of thick fat samples and PLM is the most commonly used method to visualize thin samples[82]. The birefringent nature of fat crystals make them appear bright under polarized light while the liquid oil is dark[82], which allows for clear distinction under polarized light. The advantage of PLM is that it can assess crystal structure and distribution, additionally sample preparation is simple compared to freezed- fracture SEM[4].

The fractal dimension, obtained by microscopy, describes the properties of fractal fat clusters as well as how they occupy space. In order to illustrate the principle of image analysis to obtain a fractal dimension, a two-dimensional schematic picture of

the primary crystal distribution within a cluster with size ξ is shown in Figure 9. ξ is the characteristic size of the clusters and 'a' is the diameter of the primary crystals. The maximum numbers of crystals N_m that can fit into the cluster can be expressed as:

$$N_m = \frac{\xi^2}{a^2} = (\frac{\xi}{a})^2 \quad (6)$$

Since the assumed square cluster and square lattice is not usually the case, the corrected relationship can be expressed as

$$N_m \sim (\frac{\xi}{a})^2 \quad (7)$$

And the actual number of the primary crystals embedded in this ξ size cluster N_a can be expressed as

$$N_a \sim \left(\frac{\xi}{a}\right)^D \quad (8)$$

where D is the fractal dimension. This is the model basis of particle-counting fractal dimension.

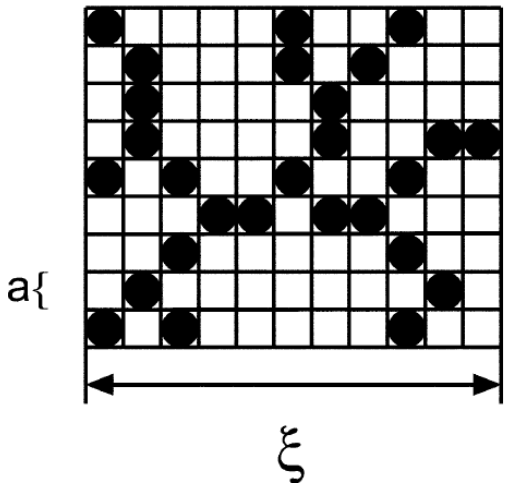

Figure 9. A two dimensional schematic representation of the primary crystal (with size a) distribution within a cluster with size ξ. Both the lattice and cluster is assumed

to be square shape for simplification. Taken from reference [82].

2.3.2.2.2.1 Particle counting fractal dimension

The particle-counting fractal dimension is determined by the relationship between the particle number in the region of interest (ROI) and the size of the region. Basically, different size boxes are laid over the PLM images (Figure 10) and the particle numbers N_p in the boxes are plotted against the corresponding square box length L in the Log-Log graph, and the slope generated is the fractal dimension D_p.

$$D_p = \frac{\Delta \ln N_p}{\Delta \ln L} \tag{9}$$

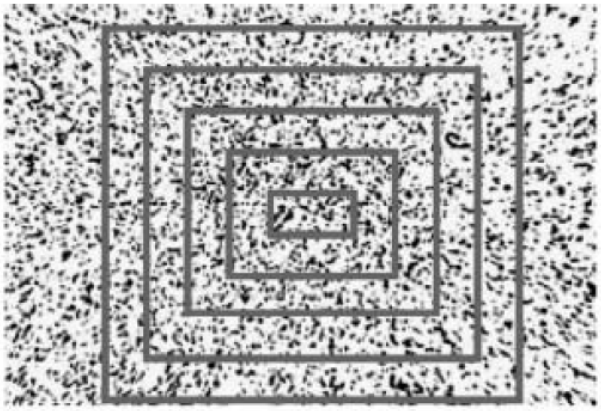

Figure 10. Particle counting procedure - different sizes of the homocentric ROI are used to obtain particle counting fractal dimension of the image. Taken from reference [79].

2.3.2.2.2.2 Box-counting fractal dimension

The box counting fractal dimension is the most commonly used method for fractal analysis on PLM images. It measures how the detail of fractal patterns changes

with the change of scale or magnification. Different sets of grids with decreasing box size are laid over PLM micrographs and the grids containing pixels of more than a certain threshold is considered to be occupied grids. The box counting fractal dimension D_b is calculated as[82]:

$$D_b = -\frac{\Delta \log N_\varepsilon}{\Delta \log \varepsilon} \quad (10)$$

where N_ε is the number of occupied grids and ε is the side length of the box. The D_b values calculated from the largest and the smallest box are exempted to reduce errors.

The fractal dimension is determined by the density of the packing of the microstructures as well as the order of their packing which are interrelated[4]. According to Tang and Marangoni [83] the box counting fractal dimension values are sensitive to crystal size and area fraction of crystal networks, while the particle-counting fractal dimension is sensitive to radical distribution patterns of the crystals.

2.3.2.2.3 Fractal dimension determined using rheological methods

The relationship between the elastic properties and the structure of different colloidal aggregates, such as aqueous polystyrene lattices, was investigated by numerous researchers since the 1980s[84-88]. The storage modulus of the fractal network G' scaled with the volume fraction of primary particles $\emptyset$ in a power law manner, described as:

$$G' \sim \emptyset^{\mu} \tag{11}$$

In 1990 Shih et al. [89] described the scaling theory of colloidal gels well above the gelation threshold, suggesting to consider the colloidal gel network as aggregations of closely packed fractal flocs which is analogous to the blobs in polymeric gel. The bond between the particles within the flocs is assumed to be a linear chain of springs, depending on the relative strength of the inner-floc links and inter-floc links, two regimes can be adopted [89](Figure 11). If the inter-floc links have a higher elastic constant than the inner-floc links, then a strong link regime is adopted[89]. The elastic constant of the system as a function of volume fraction of flocs, which is dominated by the strength of inner-floc links, has the following relationship[90]:

$$G' \sim \emptyset^{\frac{d+x}{d-D}} \tag{12}$$

where d is the Euclidean dimension of the crystal network, D is the fractal dimension of the flocs and x is the backbone fractal dimension (between 1 and 1.3). The strain at the limit of linearity σ_o in a strong link regime decreases with the increase of volume fraction in the following manner [90]:

$$\sigma_o \sim \emptyset^{-(1+d)/(d-D)} \tag{13}$$

On the other hand, in a weak link regime, the inner-floc links are stronger and the G' versus $\emptyset$ relationship changes to be[90]:

$$G' \sim \emptyset^{\frac{d-2}{d-D}} \tag{14}$$

and the limit of linearity σ_o increases with increasing volume fraction in the relationship[90]:

$$\sigma_o \sim \emptyset^{1/(d-D)} \quad (15)$$

Since the change tendency of σ_o, as a function of $\emptyset$, is opposite in the two different regimes, it is possible to determine which regime the network falls in by experimentally determining the value of σ_o.

In 1992, the same scaling theory was applied to interpreted rheological data for triglyceride aggregates and the fractal dimension calculated from the power-law dependence was in agreement with the values from light scattering experiments[80]. The relationship between small deformation rheology and the fractal dimension has widely been used to quantify the structures of various fat crystal networks in which the microstructure are considered similarly as the flocculated flocs[90]. For example the fat crystal network in the weak link regime is usually observed at high solid fat contents (~60%-100%)[91]. An schematic of idealized fat crystal network under stress is shown in Figure 12. It is also worth mentioning that the particle volume fraction $\emptyset$ is hard to measure experimentally and therefore solid fat content is used as a substitute for the volume fraction ($\emptyset_{SFC} = SFC/100$) since they are directly proportional to each other[4].

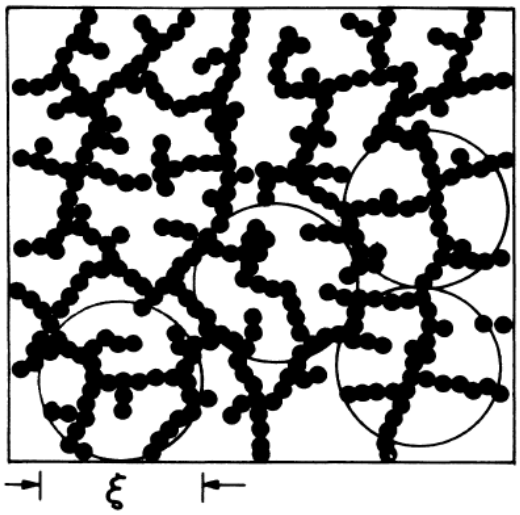

Figure 11. Schematic structure of colloidal gel where flocs are represented as circles and a have size of ξ. Taken from reference [89].

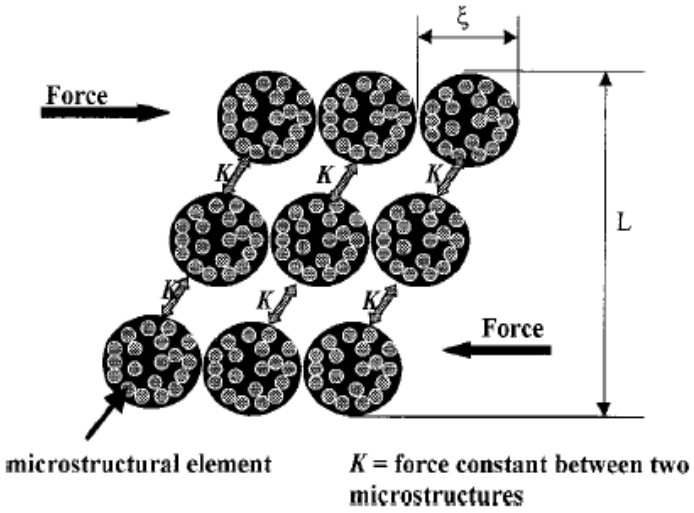

Figure 12. Schematic of an idealized fat crystal network under stress in the weak link regime. When the deformation force, which is lower than the yield stress is placed on the network, the links between the microstructure deforms while the microstructure itself remains constant in terms of its size and shape. Taken from reference [91].

2.4 Oil migration

Oil migration (or more accurately lipid migration) is typically observed in confectionery products when two or more lipid containing components are adjacent to each other[92]. It is a critical concern, especially for composite chocolate products

where chocolate is filled with fat based creams (e.g., peanut butter, nut paste) or chocolate is coated on bakery products (e.g., biscuits), since the oil migration can cause quality defects such as the softening of the chocolate, hardening of the cream filling and a greater tendency for the fat to bloom [7, 93]. In milk chocolate, the cocoa solids, milk power and sugar crystals are dispersed in a fats/oils based continuous phase, whose proportions depend on temperature [93, 94]

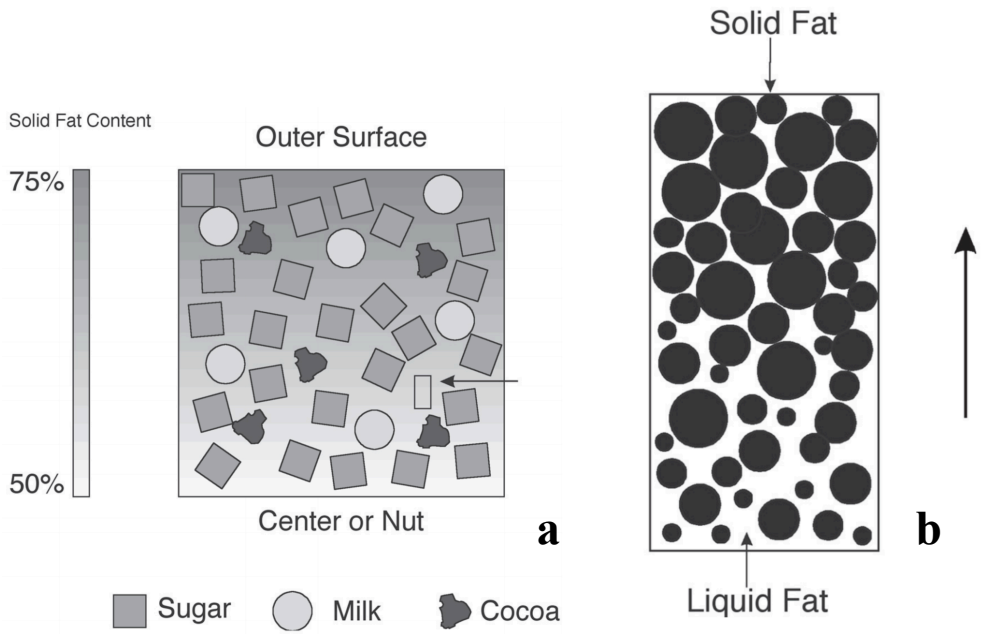

Figure 13). The softening of the chocolate is typically caused by the oil migration from the nut-based filling to the outer chocolate case[95] and fat bloom, the whitish/grayish surface, is the result of the recrystallization of cocoa butter which is usually observed during temperature fluctuations[96]. Rizan studied oil migration between dark chocolate and a hazelnut oil-based filling and found that higher temperatures accelerated fat blooming in dark chocolate because of an increased migration of foreign

triglycerides from the hazelnut filling[97].

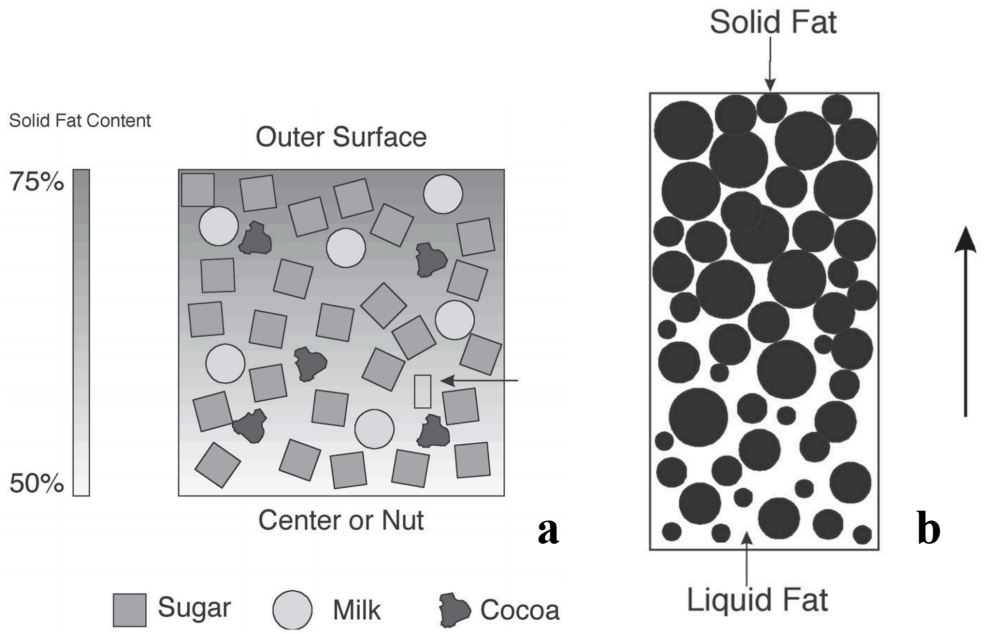

Figure 13. (a) Structure of milk chocolate where oil diffuses from an oil-containing center to the outer chocolate layer. Arrow indicates region of the lipid phase expanded in (b). (b) Expanded view of the lipid phase. Large arrow demonstrated that oil migrated from low solid content to high solid content, causing the increase of the liquid phase fraction in chocolate. Taken from reference [7] .

There are many factors that can affect fat/oil migration in chocolate which includes[7]: a) concentration gradients of the triglycerides, b) structure of the crystal matrix (e.g. crystal size, packing density, c) contact area between chocolate and filling, d) storage temperature, e) solid fat content, f) fat/oil type, g) the ratio of chocolate and fillings, and h) chocolate viscosity especially the lipid phase viscosity.

The exact fat/oil migration mechanism is not well understood however one of the preferred explanations for oil/fats migration is oil diffusion driven by the concentration gradients of the triglycerides[8]. According the Fick's first law, diffusion happens from a region of high concentration to a region of lower concentration. According to Fick's second law, the diffusion equation of unsteady-state oil migration in one-dimension can be expressed as[98]:

$$\frac{\partial c}{\partial t} = \frac{\partial}{\partial x}\left(D\frac{\partial c}{\partial x}\right) \tag{16}$$

where c is the concentration, t is time, x is the distance and D is the diffusivity depending on the nature of the substance. Diffusivity for liquids is commonly modeled by the Stokes-Einstein equation[7]:

$$\mathrm{D} = -\frac{\mathrm{kT}}{6\pi\eta\mathrm{r}} \tag{17}$$

where k is Boltzman constant (1.38×10^{-23} J K^{-1}), T is the absolute temperature (K), η is the viscosity (centipoise) and r is the molecular radius of the diffusing particle (cm). Oils/fats migration between the chocolate and fillings mainly occur through the lipid phase since the diffusivity of the triglycerides migration is significantly higher in the liquid oil compared to the solid fat[7]. When it comes to the calculation of diffusivity, the oil viscosity is estimated from the viscosity of the bulk liquid oil with lack of evidence that the oil trapped in the fat crystal network behaves in a similar fashion as bulk oil. This doubt is reasonable since researchers have shown that the microstructure of fat crystals in the matrix has a great effect on oil migration. Dibildox-Alvarado et al. studied the oil migration behavior of a mixture of peanut oil

and chemically interesterified and hydrogenated palm oil and he found that high cooling rate leads to low oil loss, because of the differences in microstructure of the fat crystal network[99].

2.5 Luminescent molecular rotors as micro-viscosity sensors

Molecular rotors are a group of fluorescent molecules composed of two or more moieties that can undergo twisted intramolecular charge transfer (TICT) upon photo excitation[100]. The moieties contain an electron-donating unit (e.g. alkylated nitrogen atom) and an electron-accepting unit (e.g. nitrile, carboxylic esters, aromatic rings) and are connected by a conjugation chain that enable the electron transfer between the donor and acceptor units[101]. After photon absorption, the excited fluorescent molecules can return to the ground state either through a locally excited state or through the TICT state[100](Figure 14). Deexcitation from the TICT state results in either a red-shifted fluorescence emission or a non fluorescent relaxation which depends on the energy gap between twisted states to ground states in twisted confirmation[35]. If the energy gap of TITC is large enough to generate photon emission, the deexcitation from TICT is radiative and exhibit a red-shifted band from the locally excited (LE) fluorescence and two fluorescent emission bands are observed[35] (Fig. 16a). One of the well-researched examples for this type of molecular rotors is 4-(Dimethylamino)Benzonitrile (DMABN). For this type of molecular rotor, the LE emission band usually shows a strong polarity-dependent solvatochromic shift and the twisted-state emission band has a strong dependence on

both polarity and viscosity[35]. Otherwise when the excited singlet state – ground sate (S_1-S_0) energy gap of twisted-state is much smaller compared to LE energy gap, the relaxation occurs nonradiatively and only one emission band is observed as in the case of 9-(dicyanovinyl)-julolidine (DCVJ) [102] (Fig. 16b). The formation rate of TICT state is lower in high viscous environments since higher viscosity commonly correlates with smaller free volume and thus high steric hindrance to the intramolecular rotation[101]. The nonradiative intramolecular rotation is competitive with the radiative decay and less formation of TICT state favors the relaxation through LE state and results in higher fluorescence intensity[101]. The fluorescence quantum yield from LE state of these single emission band molecules is viscosity-dependent, which gives molecular rotors the possibility to measure the bulk viscosity and micro-viscosity of the solvents environment. LE-state quantum yield Φ_F and viscosity of the surrounding environment, η, is found to obey a power-law relationship[35, 103]

$$\log \Phi_F = C + x \log \eta \qquad (18)$$

where η is viscosity, C and x are solvent- and compound-dependent constants. The relationship is known as the Förster-Hoffmann equation and has been proved to be valid in a broad range of polar and nonpolar fluids[104-106].

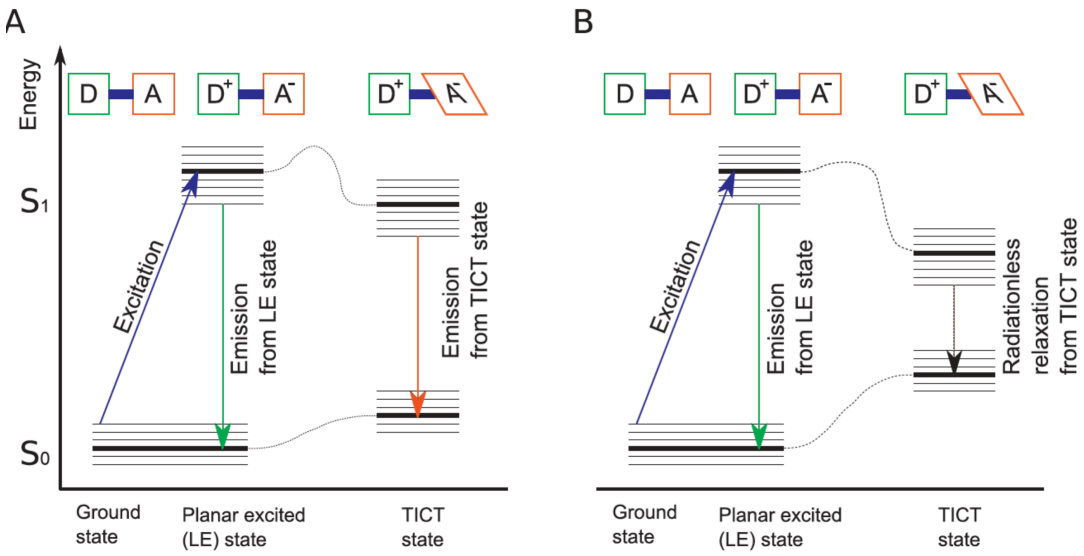

Figure 14. Extended Jabłonski diagram for molecular rotors. The excited-state energy in the TITC states is lower than in the LE state while the ground –state energy in TITC state is higher[35]. (A)If the difference of the energy gap between S_1 - S_0 energy gap is slightly lower in the TICT state than in the LE state relaxation results in a dual-band emission; (B), however, if the S_1 - S_0 energy gap is much lower than in LE state, a single-band emission is observed[35]. Taken from reference [35].

Molecular rotors acting as local viscosity probes have been recently explored in biological studies. However, the viscosity sensitivity of molecular rotor has rarely been exploited in food industry partially because the lack of information of the potential chemicals that can be used as a viscosity probes in food matrix. Ludescher et al. proposed to use mono-azo dyes (e.g., Allura Red AC, Citrus Red 2, Azorubine, Sunset Yellow and Tartrazine, Brown FK, Lithol Rubine BK, Orange B) as viscosity probes in liquid and semi-solid food matrices due to the fact that these compounds are widely used as colorants in food industry and presumptively have molecular rotor properties thus the dependency of their fluorescence quantum yield (and intensity) on solution viscosity[107](Figure 15). Abbott et al. studied the excited-state dynamics of

several non-edible mono-azo dyes and commercial azo dyes and the results suggest that non-radiative decays are predominantly observed in low viscosity solutions and that tautomerization or internal twisting are the prevalent mechanisms in non-radiative decay [108]. However, the photoexcitation dynamics of edible or GRAS azo dyes has not been well studied and the related information is very limited which is why the application of this promising viscosity probe in food industry is rarely discussed.

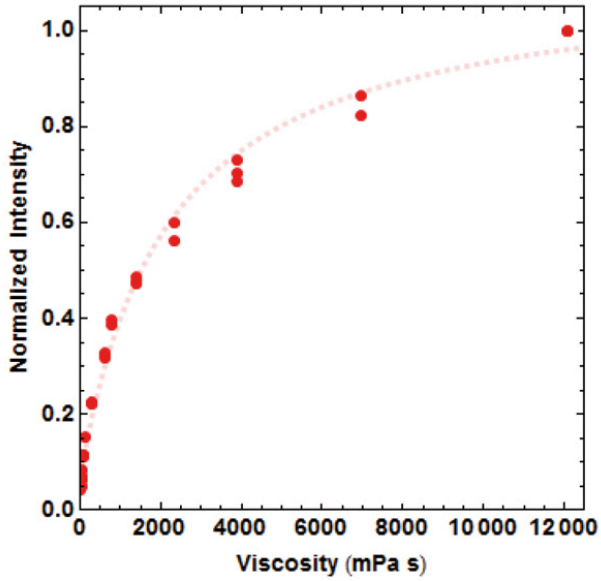

Figure 15. Dependence of fluorescence maximum intensity on viscosity for Allura Red in water-glycerol mixtures. Taken from Ludescher et al.[107]

In the following sections (section 4 and 5), all the experimental methods and results from my research will be presented in a format similar to that of the publications.

2.6 References

1. Hunter, J.E., *Dietary levels of trans-fatty acids: basis for health concerns and industry efforts to limit use.* Nutrition Research, 2005. **25**(5): p. 499-513.
2. Kromhout, D., et al., *Dietary saturated and trans fatty acids and cholesterol and 25-year mortality from coronary heart disease: the Seven Countries Study.* Preventive Medicine, 1995. **24**(3): p. 308-815.
3. Drewnowski, A., *Sensory properties of fats and fat replacements.* Nutrition Reviews, 1992. **50**(4): p. 17-20.
4. Alejandro, G.M. and S.N. Suresh, *Microstructure*, in *Fat Crystal Networks*. 2004, CRC Press. p. 179-254.
5. Wright, A.J., et al., *Solvent effects on the crystallization behavior of milk fat fractions.* Journal of Agricultural and Food Chemistry, 2000. **48**(4): p. 1033-1040.
6. Zhou, Y. and R. Hartel, *Phase behavior of model lipid systems: Solubility of high-melting fats in low-melting fats.* Journal of the American Oil Chemists' Society, 2006. **83**(6): p. 505-511.
7. Ghosh, V., G.R. Ziegler, and R.C. Anantheswaran, *Fat, moisture, and ethanol migration through chocolates and confectionary coatings.* Critical Reviews in Food Science and Nutrition, 2002. **42**(6): p. 583-626.
8. Aguilera, J.M., M. Michel, and G. Mayor, *Fat Migration in Chocolate: Diffusion or Capillary Flow in a Particulate Solid?—A Hypothesis Paper.* Journal of Food Science, 2004. **69**(7): p. 167-174.
9. Haidekker, M.A. and E.A. Theodorakis, *Molecular rotors-fluorescent biosensors for viscosity and flow.* Organic & Biomolecular Chemistry, 2007. **5**(11): p. 1669-1678.
10. Seiffert, S. and W. Oppermann, *Systematic evaluation of FRAP experiments performed in a confocal laser scanning microscope.* J Microsc, 2005. **220**(Pt 1): p. 20-30.
11. Dayel, M.J., E.F. Hom, and A.S. Verkman, *Diffusion of green fluorescent protein in the aqueous-phase lumen of endoplasmic reticulum.* Biophysical Journal, 1999. **76**(5): p. 2843-2851.
12. Damodaran, S., K.L. Parkin, and O.R. Fennema, *Fennema's food chemistry*. 4th ed. ed. 2008, Boca Raton CRC Press/Taylor & Francis.
13. Traul, K.A., et al., *Review of the toxicologic properties of medium-chain triglycerides.* Food and Chemical Toxicology, 2000. **38**(1): p. 79-98.
14. Macfarlane, S. and G.T. Macfarlane, *Regulation of short-chain fatty acid production.* Proceedings of the Nutrition Society, 2003. **62**(01): p. 67-72.
15. Diedrich, M. and K.P. Henschel, *The natural occurrence of unusual fatty acids. Part 1. Odd numbered fatty acids.* Food / Nahrung, 1990. **34**(10): p. 935-943.
16. Vlaeminck, B., et al., *Factors affecting odd- and branched-chain fatty acids in milk: A review.* Animal Feed Science and Technology, 2006. **131**(3–4): p. 389-417.
17. Craninx, M., et al., *Effect of lactation stage on the odd- and branched-chain milk fatty acids of dairy cattle under grazing and indoor conditions.* Journal of Dairy Science, 2008. **91**(7): p. 2662-77.
18. Watkins, P.J., et al., *Effect of branched-chain fatty acids, 3-methylindole and 4-methylphenol on consumer sensory scores of grilled lamb meat.* Meat Science, 2014. **96**(2, Part B): p. 1088-1094.

19. Fennema, O.R., *Food Chemistry - 3rd Edition*. 3rd ed. 1996, New York: Marcel Dekker.
20. Rottem, S. and O. Markowitz, *Unusual positional distribution of fatty acids in phosphatidylglycerol of sterol-requiring mycoplasmas.* FEBS Letters. **107**(2): p. 379-382.
21. Adam-Berret, M., A. Riaublanc, and F. Mariette, *Effects of Crystal Growth and Polymorphism of Triacylglycerols on NMR Relaxation Parameters. 2. Study of a Tricaprin−Tristearin Mixture.* Crystal Growth & Design, 2009. **9**(10): p. 4281-4288.
22. Segura, J., et al., *Effect of fatty acid composition and positional distribution within the triglyceride on selected physical properties of dry-cured ham subcutaneous fat.* Meat Science, 2015. **103**(0): p. 90-95.
23. Hu, F.B., J.E. Manson, and W.C. Willett, *Types of dietary fat and risk of coronary heart disease: a critical review.* Journal of the American College of Nutrition, 2001. **20**(1): p. 5-19.
24. Kitamura, A., et al., *High-density lipoprotein cholesterol and premature coronary heart disease in urban Japanese men.* Circulation, 1994. **89**(6): p. 2533-9.
25. Vega, G.L. and S.M. Grundy, *Hypoalphalipoproteinemia (low high density lipoprotein) as a risk factor for coronary heart disease.* Current Opinion in Lipidology, 1996. **7**(4): p. 209-16.
26. Sacks, F.M., *The role of high-density lipoprotein (HDL) cholesterol in the prevention and treatment of coronary heart disease: expert group recommendations.* The American Journal of Cardiology, 2002. **90**(2): p. 139-143.
27. Mensink, R.P., et al., *Effects of dietary fatty acids and carbohydrates on the ratio of serum total to HDL cholesterol and on serum lipids and apolipoproteins: a meta-analysis of 60 controlled trials.* The American Journal of Clinical Nutrition, 2003. **77**(5): p. 1146-1155.
28. *Dietary Guidelines for Americans, 2010*, U.S.D.o.A.a.U.S.D.o.H.a.H. Services, Editor., U.S. Government Printing Office, December 2010.: Washington, DC.
29. Assmann, G., et al., *High-density lipoprotein cholesterol as a predictor of coronary heart disease risk. The PROCAM experience and pathophysiological implications for reverse cholesterol transport.* Atherosclerosis, 1996. **124, Supplement**(0): p. S11-S20.
30. Barter, P.J. and K.A. Rye, *High density lipoproteins and coronary heart disease.* Atherosclerosis, 1996. **121**(1): p. 1-12.
31. Miller, N.E., et al., *The Tromso heart-study. High-density lipoprotein and coronary heart-disease: a prospective case-control study.* Lancet, 1977. **1**(8019): p. 965-8.
32. Abbott, R.D., et al., *High density lipoprotein cholesterol, total cholesterol screening, and myocardial infarction. The Framingham Study.* Arteriosclerosis, Thrombosis, and Vascular Biology, 1988. **8**(3): p. 207-211.
33. Lichtenstein, A.H., et al., *Dietary Fat Consumption and Health.* Nutrition Reviews, 1998. **56**(5): p. 3-19.
34. Mattson, F.H. and S.M. Grundy, *Comparison of effects of dietary saturated, monounsaturated, and polyunsaturated fatty acids on plasma lipids and lipoproteins in man.* Journal of Lipid Research, 1985. **26**(2): p. 194-202.
35. Haidekker, M.A. and E.A. Theodorakis, *Environment-sensitive behavior of fluorescent molecular rotors.* Journal of Biological Engineering, 2010. **4**: p. 11-11.
36. Greenberger, N.J. and T.G. Skillman, *Medium-Chain Triglycerides.* New England Journal of Medicine, 1969. **280**(19): p. 1045-1058.
37. Kasai, M., et al., *Effect of dietary medium- and long-chain triacylglycerols (MLCT) on accumulation of body fat in healthy humans.* Asia Pacific Journal of Clinical Nutrition, 2003.

12(2): p. 151-160.

38. Tsuji, H., et al., *Dietary medium-chain triacylglycerols suppress accumulation of body fat in a double-blind, controlled trial in healthy men and women.* Journal of Nutrition, 2001. **131**(11): p. 2853-9.
39. St-Onge, M.-P. and A. Bosarge, *Weight-loss diet that includes consumption of medium-chain triacylglycerol oil leads to a greater rate of weight and fat mass loss than does olive oil.* The American Journal of Clinical Nutrition, 2008. **87**(3): p. 621-626.
40. Tsuji, H., et al., *Dietary Medium-Chain Triacylglycerols Suppress Accumulation of Body Fat in a Double-Blind, Controlled Trial in Healthy Men and Women.* The Journal of Nutrition, 2001. **131**(11): p. 2853-2859.
41. Nosaka, N., et al., *Effects of Margarine Containing Medium-chain Triacyiglycerols on Body Fat Reduction in Humans.* Journal of Atherosclerosis and Thrombosis, 2003. **10**(5): p. 290-298.
42. St-Onge, M.P., et al., *Medium-chain triglycerides increase energy expenditure and decrease adiposity in overweight men.* Obesity Research & Clinical Practice, 2003. **11**(3): p. 395-402.
43. St-Onge, M.-P. and P.J.H. Jones, *Physiological Effects of Medium-Chain Triglycerides: Potential Agents in the Prevention of Obesity.* The Journal of Nutrition, 2002. **132**(3): p. 329-332.
44. Walstra, P., *Physical chemistry of foods.* . 2003, New York: Marcel Dekker.
45. Alejandro, G.M., *Crystallization Kinetics*, in *Fat Crystal Networks*. 2004, CRC Press. p. 21-82.
46. McClements, D.J., *Key Physicochemical Concepts*, in *Nanoparticle- and Microparticle-based Delivery Systems*. 2014, CRC Press. p. 453-522.
47. Metin, S. and R.W. Hartel, *Crystallization of Fats and Oils*. 2005: John Wiley & Sons, Inc.
48. Wright, A.J., S.S. Narine, and A.G. Marangoni, *Comparison of experimental techniques used in lipid crystallization studies.* Journal of the American Oil Chemists' Society, 2000. **77**(12): p. 1239-1242.
49. Himawan, C., V.M. Starov, and A.G.F. Stapley, *Thermodynamic and kinetic aspects of fat crystallization.* Advances in Colloid and Interface Science, 2006. **122**(1–3): p. 3-33.
50. Marangoni, A.G. and S.E. McGauley, *Relationship between Crystallization Behavior and Structure in Cocoa Butter.* Crsystal Growth Desigh, 2003. **3**(1): p. 95-108.
51. Campos, R., S.S. Narine, and A.G. Marangoni, *Effect of cooling rate on the structure and mechanical properties of milk fat and lard.* Food Research International, 2002. **35**(10): p. 971-981.
52. Avrami, M., *Kinetics of phase change. I General theory.* The Journal of Chemical Physics, 1939. **7**(12): p. 1103-1112.
53. Avrami, M., *Kinetics of phase change. II transformation‐time relations for random distribution of nuclei.* The Journal of Chemical Physics, 1940. **8**(2): p. 212-224.
54. Avrami, M., *Granulation, phase change, and microstructure kinetics of phase change. III.* The Journal of Chemical Physics, 1941. **9**(2): p. 177-184.
55. Mandelkern, L., F.A. Quinn Jr, and P.J. Flory, *Crystallization kinetics in high polymers. I. bulk polymers.* Journal of Applied Physics, 1954. **25**(7): p. 830-839.
56. Foubert, I., K. Dewettinck, and P.A. Vanrolleghem, *Modelling of the crystallization kinetics of fats.* Trends in Food Science & Technology, 2003. **14**(3): p. 79-92.
57. Marangoni, A.G. and L.H. Wesdorp, *Nucleation and Crystalline Growth Kinetics*, in *Structure and Properties of Fat Crystal Networks, Second Edition*. 2012, CRC Press. p. 27-100.

58. Ho Lam, R.S. and M.A. Rogers, *Experimental validation of the modified Avrami model for non-isothermal crystallization conditions.* CrystEngComm, 2011. **13**(3): p. 866-875.
59. Tang, D. and A.G. Marangoni, *Microstructure and fractal analysis of fat crystal networks.* Journal of the American Oil Chemists' Society, 2006. **83**(5): p. 377-388.
60. Marangoni, A. and D. Tang, *Modeling the Rheological Properties of Fats: A Perspective and Recent Advances.* Food Biophysics, 2008. **3**(2): p. 113-119.
61. Wille, R.L. and E.S. Lutton, *Polymorphism of cocoa butter.* Journal of the American Oil Chemists Society, 1966. **43**(8): p. 491-496.
62. Schenk, H. and R. Peschar, *Understanding the structure of chocolate.* Radiation Physics and Chemistry, 2004. **71**(3–4): p. 829-835.
63. Talbot, G., *Chocolate temper*, in *Industrial Chocolate Manufacture and Use*, S.T. Beckett, Editor. 1994, Springer US. p. 156-166.
64. Craven, R.J. and R.W. Lencki, *Polymorphism of Acylglycerols: A Stereochemical Perspective.* Chemical Reviews, 2013. **113**(10): p. 7402-7420.
65. Narine, S.S. and K.L. Humphrey, *A comparison of lipid shortening functionality as a function of molecular ensemble and shear: microstructure, polymorphism, solid fat content and texture.* Food Research International, 2004. **37**(1): p. 28-38.
66. Smith, P.R. and J. Johansson, *Influences of the proportion of solid fat in a shortening on loaf volume and staling of bread.* Journal of Food Processing and Preservation, 2004. **28**(5): p. 359-367.
67. Kaylegian, K.E. and R.C. Lindsay, *Performance of selected milk fat fractions in cold-spreadable butter.* Journal of Dairy Science, 1992. **75**(12): p. 3307-3317.
68. Augusto, P.E.D., et al., *Modelling the effect of temperature on the lipid solid fat content (SFC).* Food Research International, 2012. **45**(1): p. 132-135.
69. Rousseau, D., et al., *Restructing butterfat through blending and chemical interesterification. 1. Melting behavior and triacylglycerol modifications.* Journal of the American Oil Chemists' Society, 1996. **73**(8): p. 963-972.
70. Rousseau, D., A. Hill, and A. Marangoni, *Restructuring butterfat through blending and chemical interesterification. 3. Rheology.* Journal of the American Oil Chemists' Society, 1996. **73**(8): p. 983-989.
71. Rousseau, D., A. Hill, and A. Marangoni, *Restructuring butterfat through blending and chemical interesterification. 2. Microstructure and polymorphism.* Journal of the American Oil Chemists' Society, 1996. **73**(8): p. 973-981.
72. Hausdorff, F., *Dimension und äußeres Maß.* Mathematische Annalen, 1918. **79**(1-2): p. 157-179.
73. Mandelbrot, B.B., *The fractal geometry of nature* Vol. 173. 1983: Macmillan.
74. Witten, T.A. and L.M. Sander, *Diffusion-limited aggregation.* Physical Review B, 1983. **27**(9): p. 5686-5697.
75. Meakin, P., *Formation of Fractal Clusters and Networks by Irreversible Diffusion-Limited Aggregation.* Physical Review Letters, 1983. **51**(13): p. 1119-1122.
76. Kolb, M., R. Botet, and R. Jullien, *Scaling of Kinetically Growing Clusters.* Physical Review Letters, 1983. **51**(13): p. 1123-1126.
77. Weitz, D.A. and M. Oliveria, *Fractal Structures Formed by Kinetic Aggregation of Aqueous Gold Colloids.* Physical Review Letters, 1984. **52**(16): p. 1433-1436.

78. Courtens, E., et al., *Brillouin-scattering measurements of phonon-fracton crossover in silica aerogels.* Physical Review Letters, 1987. **58**(2): p. 128-131.
79. Marangoni, A.G., *The nature of fractality in fat crystal networks.* Trends in Food Science and Technology, 2002. **13**(2): p. 37-47.
80. Vreeker, R., et al., *The fractal nature of fat crystal networks.* Colloids and Surfaces, 1992. **65**(2–3): p. 185-189.
81. Narine, S. and A. Marangoni, *Fractal nature of fat crystal networks.* Physical Review E, 1999. **59**(2): p. 1908-1920.
82. Tang, D. and A. Marangoni, *Microstructure and fractal analysis of fat crystal networks.* Journal of the American Oil Chemists' Society, 2006. **83**(5): p. 377-388.
83. Tang, D. and A. Marangoni, *Computer simulation of fractal dimensions of fat crystal networks.* Journal of the American Oil Chemists' Society, 2006. **83**(4): p. 309-314.
84. Buscall, R., et al., *Scaling behaviour of the rheology of aggregate networks formed from colloidal particles.* Journal of the Chemical Society, Faraday Transactions 1: Physical Chemistry in Condensed Phases, 1988. **84**(12): p. 4249-4260.
85. Kantor, Y. and I. Webman, *Elastic Properties of Random Percolating Systems.* Physical Review Letters, 1984. **52**(21): p. 1891-1894.
86. Sonntag, R.C. and W.B. Russel, *Elastic properties of flocculated networks.* Journal of Colloid and Interface Science, 1987. **116**(2): p. 485-489.
87. Bremer, L.G.B., et al., *Formation, properties and fractal structure of particle gels.* Advances in Colloid and Interface Science, 1993. **46**(0): p. 117-128.
88. Bremer, L.G.B., et al., *On the fractal nature of the structure of acid casein gels.* Colloids and Surfaces, 1990. **51**(0): p. 159-170.
89. Shih, W.-H., et al., *Scaling behavior of the elastic properties of colloidal gels.* Physical Review A, 1990. **42**(8): p. 4772-4779.
90. Narine, S.S. and A.G. Marangoni, *Relating structure of fat crystal networks to mechanical properties: a review.* Food Research International, 1999. **32**(4): p. 227-248.
91. Narine, S.S. and A.G. Marangoni, *Mechanical and structural model of fractal networks of fat crystals at low deformations.* Physical Review E, 1999. **60**(6): p. 6991-7000.
92. Couzens, P. and H. Wille, *Fat migration in composite confectionery products.* Manufacturing Confectioner, 1997. **77**: p. 45-7.
93. Ziegler, G.R., A. Shetty, and R. Anantheswaran, *Nut oil migration through chocolate.* The Manufacturing Confectioner, 2004. **84**(9): p. 118-126.
94. Aguilera, J.M., D.W. Stanley, and K.W. Baker, *New dimensions in microstructure of food products.* Trends in Food Science & Technology, 2000. **11**(1): p. 3-9.
95. Widlak, N., R. Hartel, and S. Narine, *Crystallization and solidification properties of lipids*. 2001: AOCS Press.
96. Hartel, R.W., *Chocolate: fat bloom during storage.* Manufacturing Confectioner, 1999. **79**: p. 89-99.
97. Khan, R.S. and D. Rousseau, *Hazelnut oil migration in dark chocolate – kinetic, thermodynamic and structural considerations.* European Journal of Lipid Science and Technology, 2006. **108**(5): p. 434-443.
98. Cussler, E.L., *Diffusion: mass transfer in fluid systems*. 2009: Cambridge university press.
99. Dibildox-Alvarado, E., et al., *Effects of Crystalline Microstructure on Oil Migration in a*

Semisolid Fat Matrix. Crystal Growth & Design, 2004. **4**(4): p. 731-736.

100. Haidekker, M.A., et al., *Dyes with Segmental Mobility: Molecular Rotors*, in *Advanced Flourescence Reporters in Chemistry and Biology I: Fundamentals and Molecular Design*, A.P. Demchenko, Editor. 2010. p. 267-308.
101. Uzhinov, B.M., V.L. Ivanov, and M.Y. Melnikov, *Molecular rotors as luminescence sensors of local viscosity and viscous flow in solutions and organized systems.* Russian Chemical Reviews, 2011. **80**(12): p. 1179-1190.
102. Allen, B.D., et al., *The photophysical properties of a julolidene-based molecular rotor.* CCPhysical Chemistry Chemical Physics, 2005. **7**(16): p. 3035-40.
103. Forster, T. and G. Hoffmann, *Die Viskositatsabhangigkeit der Fluoreszenzquantenausbeuten einiger Farbstoffsysteme [Effect of viscosity on the fluorescence quantum yield of some dye systems].* Zeitschrift für Physikalische Chemie, 1971. **75**: p. 63 - 76.
104. Haidekker, M.A., et al., *Effects of solvent polarity and solvent viscosity on the fluorescent properties of molecular rotors and related probes.* Bioorganic Chemistry, 2005. **33**(6): p. 415-425.
105. Nipper, M.E., et al., *Characterization of changes in the viscosity of lipid membranes with the molecular rotor FCVJ.* Biochimica Et Biophysica Acta-Biomembranes, 2008. **1778**(4): p. 1148-1153.
106. Law, K., *Fluorescence Probe for Microenvironments: Anomalous Viscosity Dependence of the Fluorescence Quantum Yield of P-N, N Dialkylaminobenzylidenmalononitrile in 1-Alkanols.* Chemical Physics Letters, 1980. **75**(3): p. 545 - 549.
107. Ludescher, R.D. and M.G. Corradini, *Monoazo dyes as probes for bulk and local viscosity - Potential applications in semi-solid foods.* Agro Food Indusrty Hi Tech 2012. **23**(3): p. 12-14.
108. Abbott, L.C., et al., *Picosecond deactivation of azo dye excited states in solution and in cellulose.* Journal of Photochemistry and Photobiology A: Chemistry, 2011. **218**(1): p. 11-16.

3 Physico-Chemical Properties of Tristearin-Oil Blends: The Influence of Long-Chain Unsaturated and Medium Chain Triglycerides

3.1 Abstract:

The chemical structure of the liquid oil plays a critical role in influencing the crystallization process of hardstock fats, namely tristearin. Medium chain triglycerides and unsaturated oils alter the crystallization of tristearin differently with respect to their kinetics, microstructure as well as phase behavior. Irrespective of the unsaturated triglyceride and dilution factor used, the mode of nucleation remained instantaneous, while for medium chain triglyceride the mode of nucleation changed from instantaneous to sporadic nucleation when tristearin was diluted beyond 70 wt% oil. Since these factors are strongly related to the mechanical and thus sensory properties of the fat blends, it is possible to manipulate the structure of the solid fats by incorporating different types of oils that may change the properties of the hardstock fat.

3.2 Introduction:

Fats play critical roles in many foods providing ‘solid-like’ elastic structure that alter sensory properties ranging from mouth-feel, hardness to spreadability [1-6]. More often, the physical chemistry of oil based foods are studied from the perspective of the solid fat as opposed to the liquid oil even though it has been shown that the oil solvents influence crystallization processes of solid fat, other than the obvious dilution effects [2, 7]. However, the mechanisms for this phenomenon are not fully understood

since most studies focus on natural lipids that contain complex profiles of triglycerides. As an example, the high melting fraction of milk fat are usually used as a model solid fat while the low melting fraction of milk fat, canola oil as well as soybean oil are typically used as oil solvents. It is difficult to determine cause-and-effect relationships in such complex systems. This is why herein we systematically modify the oil triglycerides in order to understand the most basic relationships between their structures and the effects on crystallization of solid fat.

It is well know that excessive consumption of fats, especially saturated and *trans* fats are correlated to cardiovascular disease [8] while recent studies show that the replacement of saturated fat with polyunsaturated and/or monounsaturated lipids lower the associated risk of coronary vascular disease, more efficiently than reducing overall fat intake [9, 10]. As well, medium chain triglycerides (MCTs) have demonstrated some beneficial effects from an obesity perspective, which are also related to the excessive energy intake partially due to high fat consumption. Studies have illustrated that MCTs have potential in suppressing accumulation of body fat and may help control body weight [11-13]. Accordingly, in this study, two types of liquid oils, unsaturated, long-chain triglycerides and saturated medium-chain triglycerides, were chosen as oils in this study. This study aims at using a simplified system to understand how differences in oil structure impacts the crystallization of solid fat, tristearin, with regards to the crystallization kinetics, solids content, and fractal nature of the corresponding colloidal fat crystal networks.

3.3 Materials and Method

3.3.1 Sample Preparation

Two unsaturated long-chain triglycerides (ULCTs) (Triolein and Trilinolein) and four saturated medium-chain triglycerides (MCTs) (Tricaprin, Tricaprylin, Tricaproin, Tributyrin) were selected as liquid oils for the experiment. Tristearin was used as the solid fat and blended with each of oil, at various weight percentages (10%, 20%, 30%, 40%, 50%, 60%, 70%). The mixtures of tristearin and solvent were heated at 100℃ for 20 min to ensure that the two components were melted and homogeneous. The mixtures were then stored at 4℃ until use.

3.3.2 Melting and Crystallization Behavior (DSC)

Differential scanning calorimetry (DSC) Q2000 (TA Instruments, New Castle, Delaware, USA) was used to study the melting and crystallization behavior of the blended fats at different solid-liquid fats ratios. 5-10 mg of each blended fat were hermetically sealed in aluminum DSC pans and melted at 100 ℃ for 20 minutes. Samples were then transferred into incubators set at 35 ℃ for 24 hrs. Samples were then heated from 35 ℃ to 120 ℃ at 20 ℃/min, then equilibrated at 120 ℃ for 5 min and finally cooled to 35 ℃ at 2 ℃/min. During the melting and crystallization cycles, thermograms were recorded and analyzed using Universal Analysis 2000 software (TA Instruments, New Castle, Delaware). The onset temperature for both

crystallization and melting were measured using the inflection point on the thermograms [2]. A running integral was applied to the crystallization peak and the integration curve (i.e. crystal volume fraction vs. time data) was obtained and fitted to the modified Avrami model [14]. Three replicates were performed for each sample by going through the heating and cooling cycles three times each separated by a 24 hr incubation time at 35℃.

3.3.3 Polarized Light Microscopy (PLM)

Samples, microscope glass slides, cover slips and transfer pipettes were heated to 100 ℃ for 30 min. A small droplet of the melted fat was placed on a glass slide and a glass cover slip was placed on top immediately ensuring that the sample thickness was uniform [1]. The slides were transferred into incubators set at 35 ℃ for 24 hrs. A light microscope was used to observe samples under polarized light at low magnification using a 10 × lens (Olympus, Tokyo, Japan). Samples were placed in a temperature-controlled Peltier stage (Linkam Scientific Instruments, UK) and the temperature was held at 35℃. Images were obtained with a Q Imaging camera equipped with QCapture Pro 7 computer software (QImaging, Surrey, BC, Canada). For each sample, six images at different locations were taken and results were averaged. Image J 1.47v (Wayne Rasband, National Institutes of Health, USA) was used for advanced image analysis. The color contrast of the images was first adjusted at the level that all the microstructures were clearly represented and the images were then converted to binary type. This was followed by a box-counting fractal technique

and a fractal dimension was calculated using the FracLac plug-in.

3.3.4 Small Deformation Rheology

The samples and glass pipettes used to transfer the samples were heated at 100 ℃ for 30 min. The melted samples were transferred into plastic molds producing disks of fat (19 mm in diameter and 3mm thick) and were stored at 35 ℃ for 24 hrs. A Discovery HR2 Hybrid Rheometer (TA Instruments, New Castle, DE, USA) was used to perform small deformation rheology using a controlled stress. After incubation, the samples were transferred between an 8 mm diameter stainless steel cross-hatched geometry and a cross-hatched parallel Peltier plate maintained at 35℃. The gap was controlled using a controlled normal force between 2 and 5 N to ensure sufficient contact between the geometry, the sample and the plate to prevent slippage. This was used in place of a controlled gap with slight compression because the phase volume of the solids differed drastically between samples. An oscillatory stress sweep was performed between 2 Pa to 500 Pa (within linear viscoelastic region) at 1 Hz. Three replicates were performed for each fat blend.

3.3.5 Pulsed Nuclear Magnetic Resonance Spectroscopy (Solid fat content)

A Bruker mq20 Series NMR analyzer (Bruker, Milton, Ontario, Canada) was used to measure the free induction decay and T_2 relaxation of the solid crystalline fraction with a Hahn-echo pulse sequence [15, 16]. The pulse length at 90 ° was set to

2.5 μs and 5.1 μs which are typical for solids measurements. The gain (64) and recycle delay (5 sec) were obtained and Tau was selected to be 0.5 ms which was as short as possible to reduce the diffusion and chemical exchange.

3.4 Result & Discussion

The crystallization kinetics, examined using DSC has numerous advantages: precise temperature control, uniform temperature throughout the sample, elimination of potential presence of foreign nuclei due to the relative small sample size [17] and high sensitivity to evolution of heat released during lipid crystallization process [18-21]. At high tristearin/oil ratios, the DSC thermograms of the blended fats displayed a single exothermic peak (Figure 1A) that was integrated using a running integral to obtain phase volume vs. time profile. At low tristearin/ oil ratios, two peaks were observed (Figure 1B) which may occur due to a transition between polymorphic forms or a two stage crystallization [22] and in this case the integration was completed across both peaks since the two peak were not resolved (i.e., the minimum did not reach base line). The integrated phase volume was fitted to the non-isothermal Avrami model:

$$\frac{\mathrm{V}}{V_m} = 1 - e^{-k(t-Z)^n} \quad (1)$$

where V is the phase volume of the crystals at time t, V_m is the maximum crystal volume attained after the completion of crystallization, $\frac{\mathrm{V}}{V_m}$ is the phase volume integrated from DSC exothermic peak, k is Avrami constant (aka rate constant of crystallization), n is the Avrami exponent and Z is the induction time. This model was

developed to characterize crystallization events and is often used to characterize fat crystallization kinetics [17]. The model is generally defined as a sigmoidal process that is characterized by a lag-period, initially during the formation of crystal embryo, followed by a rapid increase in crystal phase volume and finally a plateau when all the lipid molecules are crystalized out and equilibrium was achieved [23]. The integration curve of the crystallization peak, which is $\frac{V}{V_m}$ as a function of time t, is fitted into the Avrami model.

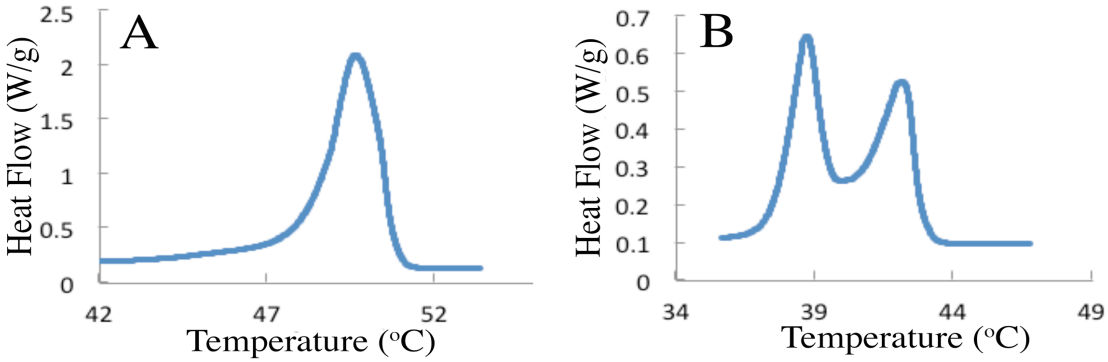

Figure 1: DSC crystallization exotherms of (A) low, 10% tributyrate/ 90% tristearin blends, and (B) high, 70% triolein/ 30% tristearin blends.

The Avrami rate constant, k, increases with a decrease in the solid tristearin mass ratio irrespective of the liquid oil (Figure 2). This indicates an elevated concentration of oil accelerates the rate of nucleation, rate of crystal growth or both. Unfortunately, since k depends on both factors more definitive information cannot be ascertained [17]. This observation may partially be explained by: 1) a decrease in solution viscosity during latter stages of crystallization making it easier for the diffusion of tristearin to the surface of the growing crystal and thus an increase in the rate constant

of crystal growth, and/or 2) the change in the mode of nucleation (e.g., from sporadic to instantaneous). It is not surprising that the rate constant increases as the dissimilarity between the oil and tristearin increases (i.e., shorter chain saturates (C4-C8) compared to longer chain saturated oils (C10) and polyunsaturated (18:2) versus monounsaturated (18:1)). If k is changing solely as a result of an increase in the chemical potential, an inverse correlation should be observed between induction time, Z, and molecular similarity between the oil and tristearin.

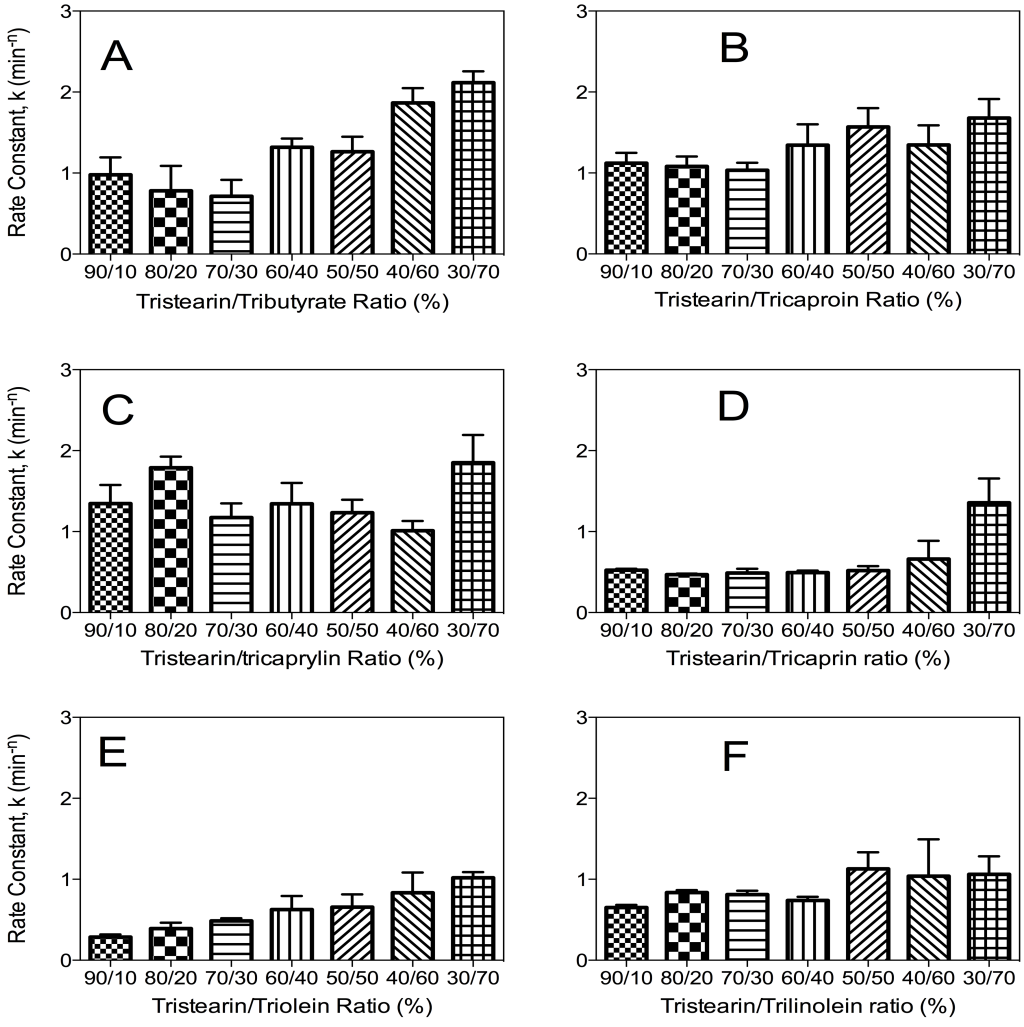

Figure 2: Changes of Avrami constant as a function of mass ratio of tristearin in fat blended system.

Similar increasing trends were also observed between the induction time, Z, and the tristearin/oil ratio (Figure 3). Induction time was insensitive to the chemistry of the oil (i.e., MCTs or unsaturated oil) compared to k therefore it cannot be concluded that the molecular dissimilarity accounts for all the changes in k. As the dilution of tristearin with oil increased there was an increase in the time of undercooling required for nucleation from between 6 and 7 min to between 8 and 9 min. The dilution effect of the liquid oil made it harder for the formation of the stable nucleus that resulted in the delay of the starting point of the nucleation.

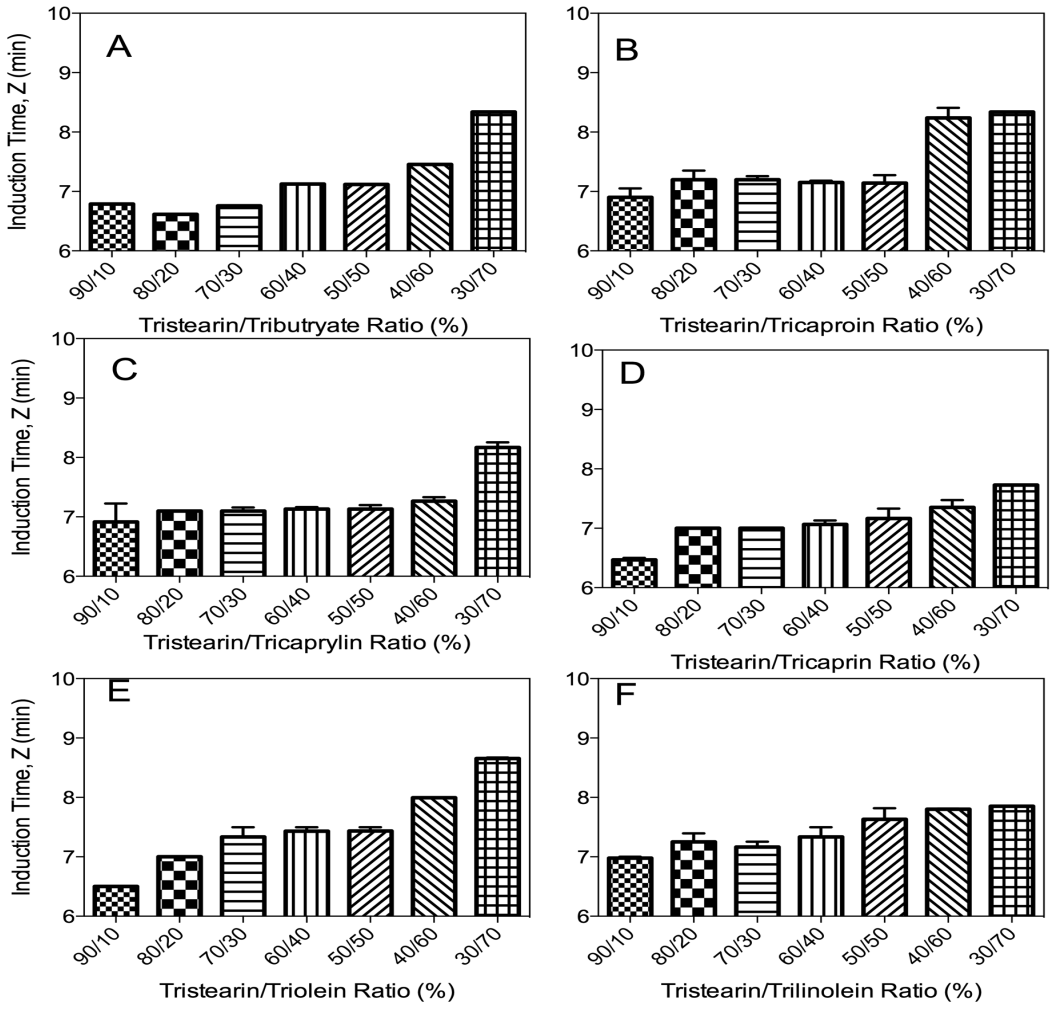

Figure 3: Induction time, z, determined by fitting the Avrami model to the integrated DSC crystallization exotherm, as a function of mass ratio of tristearin.

The Avrami exponent, n, represents both the mode of nucleation (instantaneous & sporadic) and dimensionality of crystal growth (rod-like, disc-like & spherulitic) (**Error! Reference source not found.**)[23]. The relationship between the magnitude of n and the nucleation mode and growth mechanism is demonstrated in Table 1. If n is equal to 2 or 3, the mechanisms of nucleation and growth are not exclusive to a single set of parameters and the mode of crystal growth is typically determined using microscopy. It should also be mentioned that although theoretically n should be an integer between 1 and 4, non-integer values are frequently observed from experimental results. Numerous mechanism for non-Euclidian values have been suggested including [23, 24]: (a) the simultaneous presence of two types of crystals and/or the existence of both sporadic and instantaneous nuclei in the system, (b) the growth rate changes during the crystallization process, (c) the contraction of the fats during supercooling, and (d) the growth rate changes during the process. At oil ratio below 30%, the Avrami exponent value remained constant for each of the six fats blends (~3) indicating that either instantaneous nucleation with spherulitic crystal growth or sporadic nucleation with disc-like crystal growth occurred.

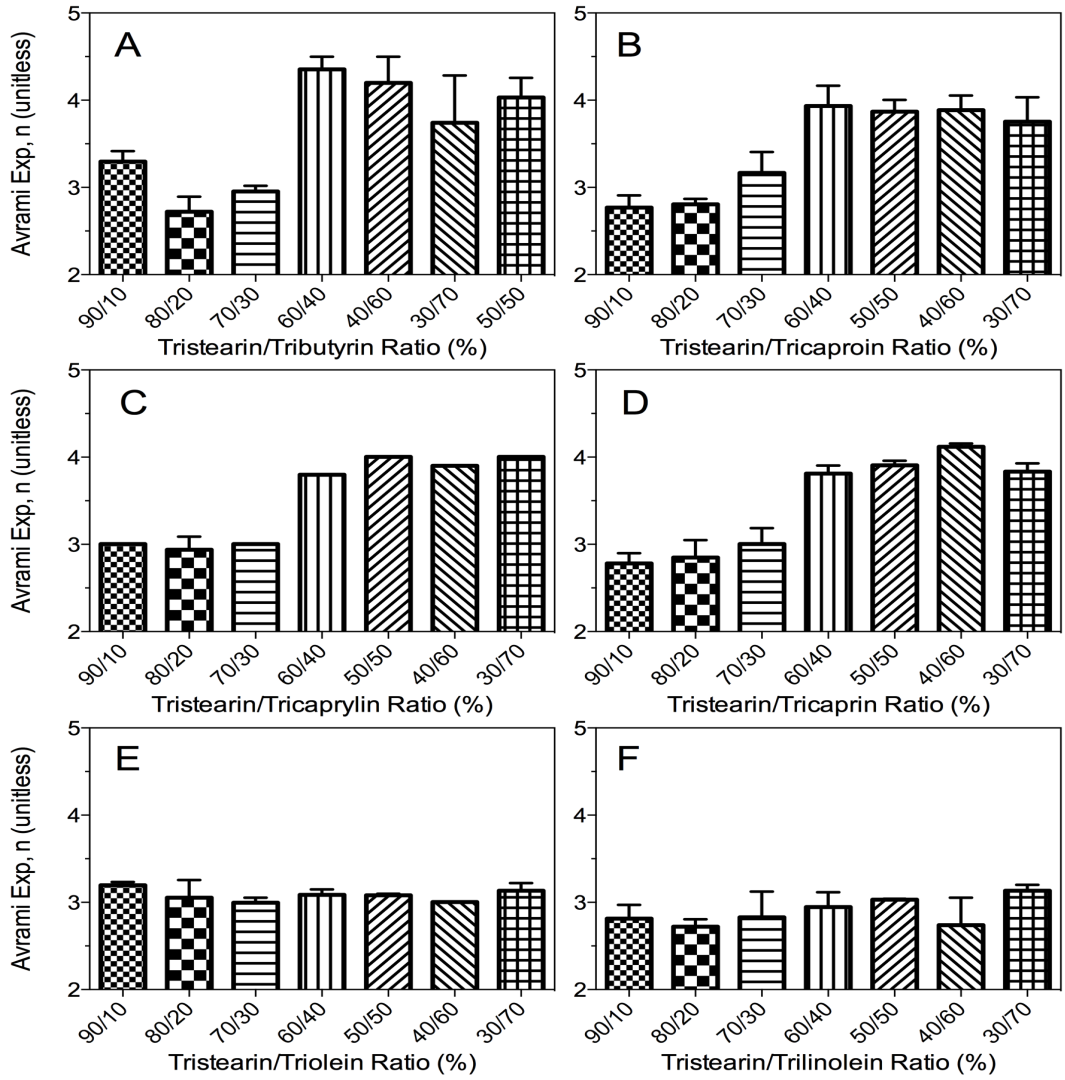

Figure 4: Avrami Exponent, n, determined by fitting the Avrami model to the integrated DSC crystallization exotherm, as a function of mass ratio of tristearin.

Table 1. Avrami exponent n for different nucleation mode and crystal growth model.

Nucleation mode	Crystal growth mode	Avrami exponent n
Instantaneous (0)	Rod-like (1)	0+1=1
Instantaneous (0)	Disc-like (2)	0+2=2
Instantaneous (0)	Spherulitic (3)	0+3=3
Sporadic (1)	Rod-like (1)	1+1=2
Sporadic (1)	Disc-like (2)	1+2=3
Sporadic (1)	Spherulitic (3)	1+3=4

In order to determine the nucleation and growth mechanism, micrographs of the tristearin oil blends were obtained. For all samples Maltese crosses are observed under polarized light (Figure 5, 6), which confirmed that the crystal growth was spherulitic [23]. Therefore, the nucleation mode is instantaneous when n ~ 3. For the 4 MCTs n changed to 4 at high oil concentration (>40%), which indicated nucleation mode change from instantaneous to sporadic at high dilution level. While for triolein and trilinolein the nucleation mode remained to be instantaneous no matter what is the tristearin/oil ratio. It is extremely interesting to note that the mode of nucleation changed when diluted with MTCs but not with long chain unsaturated oils.

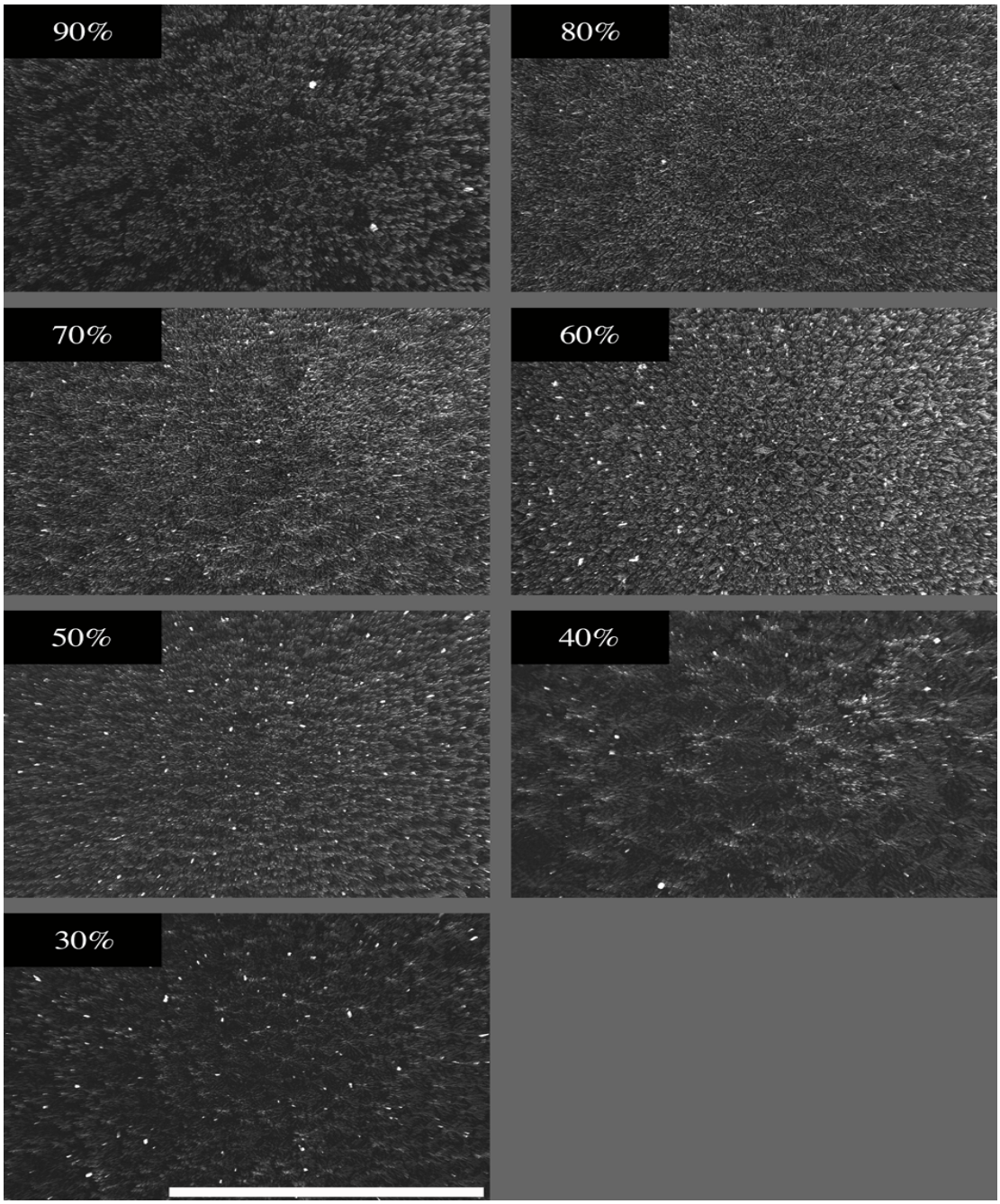

Figure 5: Polarized light micrographs of tristearin/tributyrate blends. Magnification bar = 100μm.

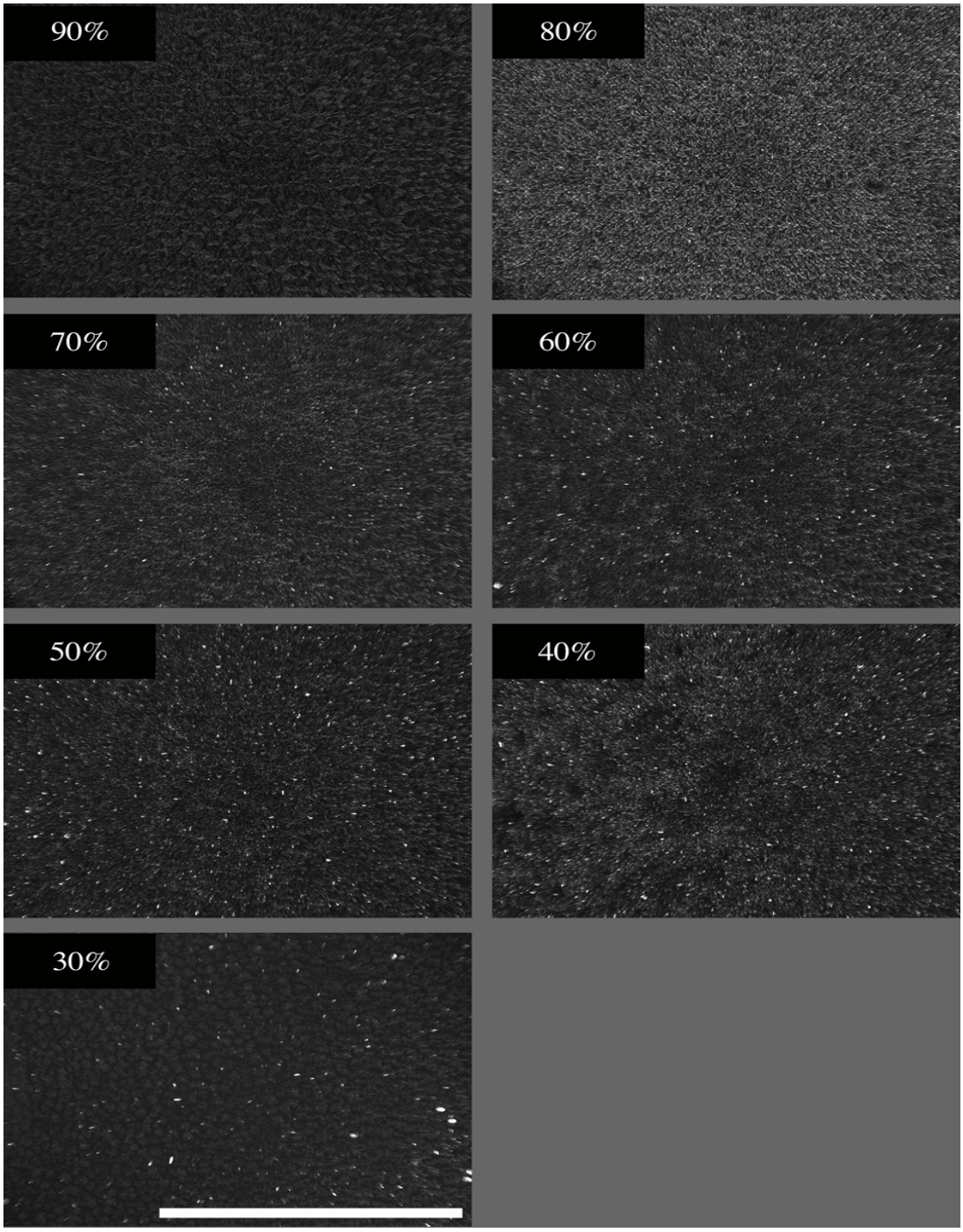

Figure 6: Polarized light micrographs of tristearin/Trilinolein blends. Magnification bar = 100μm.

It is clear that MTCs and unsaturated oils alter the crystallization kinetics differently, at dilutions greater than 60/40 tristearin/oil; however, how the difference impact the mechanical properties that are closely related to the sensory attributes

remains undefined. Numerous levels of structures, in fat crystal networks, ranging from the primary crystals, clusters and the final macroscopic 3D fat crystal network are all central in defining the microstructure of the material [25, 26]. It is often proposed that fat crystal networks contain a self-similar character and the microstructure may be described in terms of its fractal nature. So fractal dimensions are commonly used as an indicator for the scaling of the microstructures. Herein, both a box-counting microscopy fractal dimension and rheological fractal dimension were used.

The microscopy fractal dimension was established using a box-counting method (D_b) over particle counting (D_p) and Fourier-transform methods (D_f) since Tang et al. [27] demonstrated that D_b is sensitive to both the crystal size and area fraction while D_p is sensitive to the radial density and D_f is only sensitive to crystal size. For each blended sample, at specific mass ratios, six micrographs were taken and D_b was calculated for the average of the six blends (Figure 7). Clearly, it may be seen that for the four MCTs blends, D_b increased dramatically with an increase in the tristearin/oil ratio to 70/30 where it then plateaued. While for triolein and trilinolein blends, there was no change of D_b across all tristearin/oil ratios. Accordingly, the increasing D_b trend for MCTs is either because of an increase in crystal size and/or more densely packed crystals [27]. The same scenario was not observed for tristearin blends with unsaturated oils where no major changes in D_b were observed, correlating well to the observations made with the Avrami parameters (Figures 2-4). Since many factors

influence its microstructure, it is difficult to define the cause of the differences observed between unsaturated oils and MCTs.

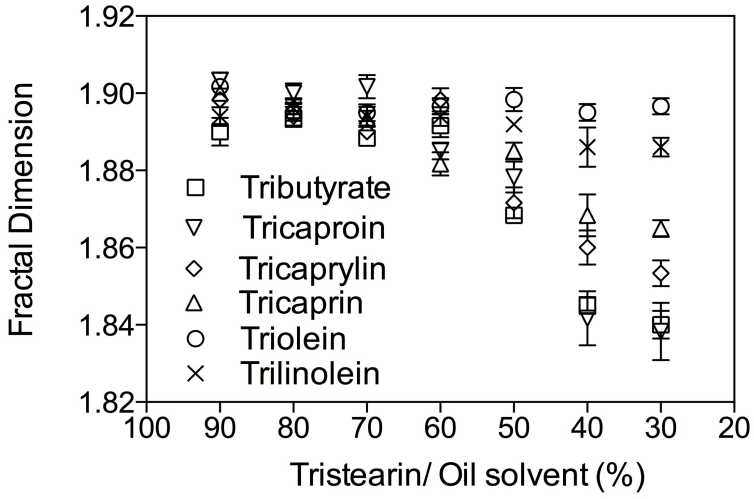

Figure 7: The box counting fractal dimension at different tristearin concentration for different unsaturated and MCT oil blends.

The physical fractal dimension, obtained using small deformation rheology, has been used as an indicator to relate structural elements in colloidal gel networks to its mechanical properties [28] that was later extended to fat crystal networks by Vreeder [29]. The explanation of the theory was discussed in chapter 2.3.2.2.3. The relationship between G′ and tristearin concentration φ in different liquid oils obeyed a power law trend as described in equation (2) and was linearized using a log-log relationship (Figure 8). The slope of these linearized plots is the exponential term μ and is used to acquire D calculated by both equation (3) for weak-link regime and equation (4) for strong-link regime[3]. (d is the Euclidean dimension of the crystal network, D is the fractal dimension of the crystal clusters and x is the backbone fractal dimension.)

$$G' \sim \varphi^{\mu}, \quad (2)$$

$$\mu = \frac{d-2}{d-D}, \quad (3)$$

$$\mu = \frac{d+x}{d-D}, \quad (4)$$

Table 2. Physical Fractal dimension (D) calculation for both Weak-link Regime and Strong-link Regime

Oil	Slope	R^2	WLF	SLF
Tributyrin	3.03	0.93	2.67	1.68
Tricaproin	3.16	0.90	2.68	1.73
Tricaprylin	3.08	0.96	2.67	1.70
Tricaprin	3.17	0.95	2.68	1.74
Triolein	3.91	0.95	2.75	2.00
Trilinolein	3.90	0.93	2.75	2.00

WLF is weak link fractal dimension; SLF is strong link fractal dimension.

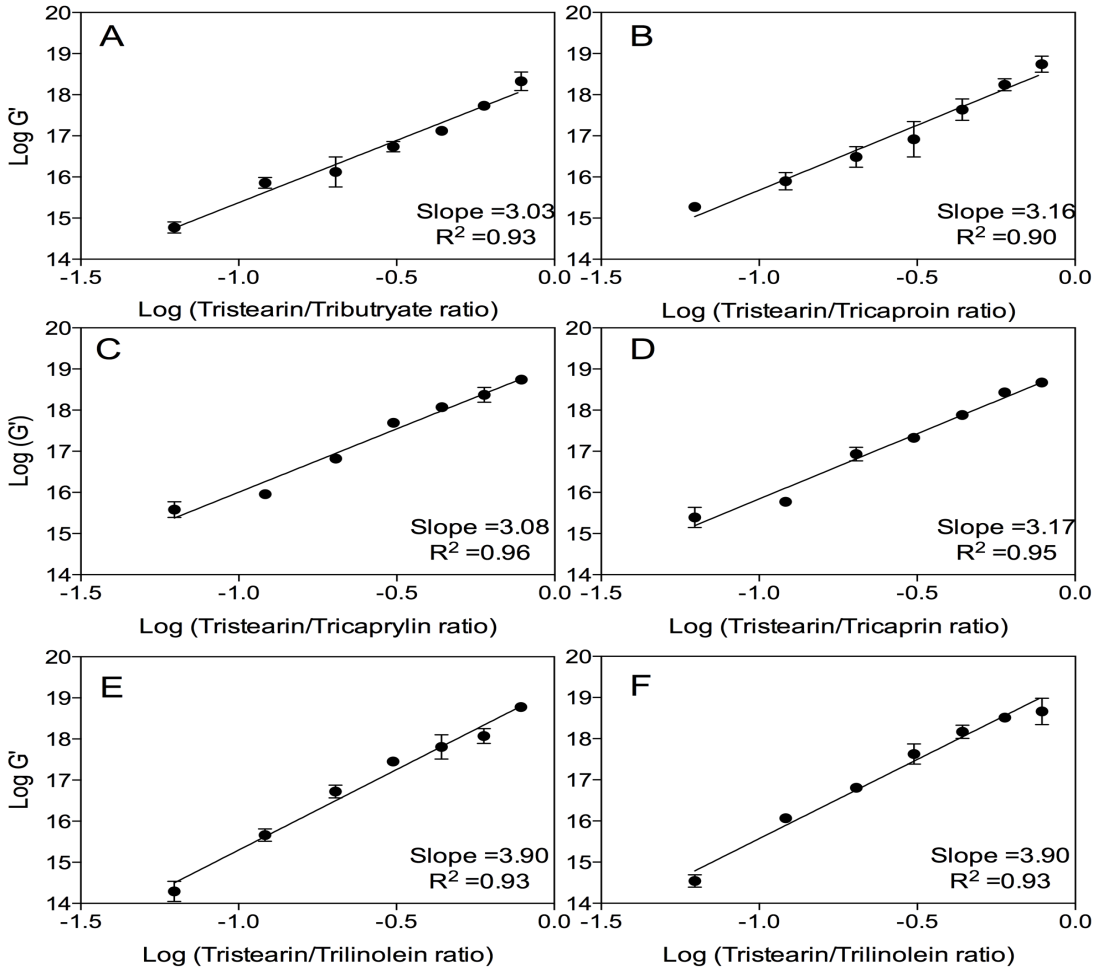

Figure 8: The relationship between the storage modulus (G') and the volume fraction of tristearin in the different unsaturated and oils.

The D value, irrespective if it is calculated from the strong-link or weak-link regimes, shared the similar features (Table 2). A fractal dimension of 2 was observed for both unsaturated oil blends. The four MCTs blends were statistically the same; however, the values between the two types of oils were significantly different. This indicates that the two types of oils led to different microstructures. For both rheological and box counting fractal dimensions, the unsaturated oil blends were higher than the fractal values for the MCTs oil blends.

The inverse of the onset temperature for melting, as a function of tristearin ratio for six different fat blends, which ranged between 55 to 70 ^{o}C, was used to approximate if ideal solubility was followed during the dilution of tristearin (Figure 9). The solid line in Figure 9, represents the ideal solubility of triglycerides obtained using the Hildebrand solubility equation [4]:

$$\log_{10} X = \frac{\Delta H}{R}\left(\frac{1}{T_m} - \frac{1}{T_b}\right), \quad (5)$$

where X is the mole fraction of the high melting point lipid which is approximate to be the mass fraction of tristearin in our experiment, R is the universal gas constant (8.314J/$mole^{-1}kg^{-1}$), ΔH is the enthalpy of tristearin (J/mole), T_m is the melting point (K) of tristearin and T_b is the melting point (K) of the fat blends. The theoretical T_b value was calculated (represented as the solid line in Figure 9) at each mass fraction X. By comparing the experimental results to the solid ideal solubility line, it was observed that the blends of tristearin and unsaturated oils closely follow ideal solubility, sharing very similar slopes. However, MCTs blends deviated from ideal solubility suggesting that the MCTs do not simply act as a diluting oil.

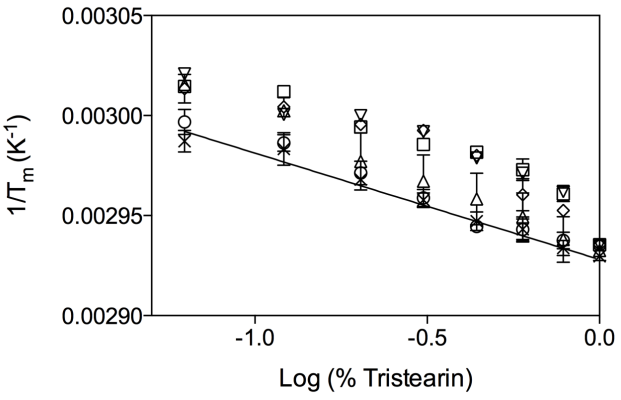

Oil Phase	Slope (10^{-5})	R^2
□ Tributyrate	-6.04 ±0.4	0.88
▽ Tricaproin	-6.05±0.5	0.90
◇ Tricaprylin	-6.23 ±0.5	0.85
△ Tricaprin	-7.14 ±0.7	0.80
○ Triolein	-5.42 ±0.2	0.87
× Trilinolein	-5.15 ±0.4	0.85
— Ideal	-5.31 ±0.2	1.00

Figure 9: The relationship between the inverse of the melting temperature and the

log of the tristearin concentration for each of the six oil blends. Solid line represents the theoretical ideal solubility calculated from eq. 5.

In order to observe if there is an effect, other than a simple dilution, of the different oils on the crystallization of tristearin, the solid fat content (SFC) was measured using pNMR for six systems (Figure 10). The solid line represents the ideal solubility of tristearin in each of the oils where the SFC is exactly equal to the % tristearin added whereby the SFC is determined simply by its colligative properties. From the fitted slopes it is clear that the unsaturated oils follow ideal solubility while the MCTs oils tended to have higher SFC value than predicted corresponding well with observations made with the melting behavior (Figure 9). The deviation of the slope from the ideal solubility line for tristearin/MCTs blends is possibly because the formation of co-crystals between MCTs and tristearin [30]. The MCTs may pack more effectively with tristearin enabiling co-crystalization in the blends. This may arise because of a similarity of molecular configuration between MCTs and tristearin. For the triolein and trilinolein, although they have the same carbon chain length as tristearin, the double bond in the carbon chain may prevent them from effectively packing into the tristearin lattice. That also may explain the change of Avrami exponent, n. At high oil concentrations, the nucleation for MCTs system changes from instantaneous to sporadic while unsaturated oils did not alter the mode of crystallization and thus the nucleation of tristearin remained instantaneous.

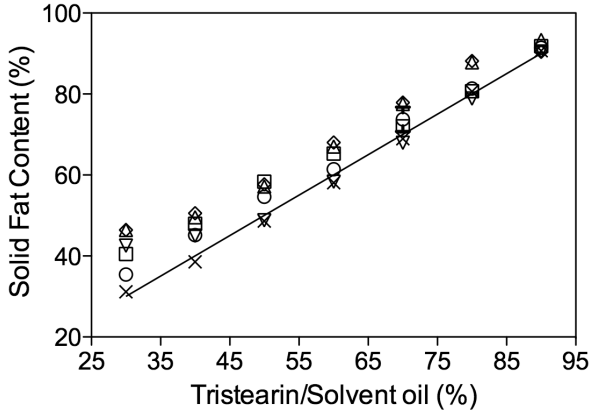

Oil Phase	Slope	R^2
□ Tributyrate	0.83 ±0.01	0.995
▽ Tricaproin	0.82 ±0.04	0.955
◇ Tricaprylin	0.81 ±0.03	0.979
△ Tricaprin	0.85 ±0.03	0.983
○ Triolein	0.96 ±0.02	0.999
× Trilinolein	1.01 ±0.01	0.996
—— Ideal	1.00 ±0.00	1.000

Figure 10: The relationship between solid fat content and tristearin concentration. Solid line represents the theoretical ideal solubility.

3.5 Conclusions

From the results and analysis above, it can be concluded that the chemical structure of the diluting oil plays a critical role in influencing the crystallization process. The MCTs and the unsaturated oils affect the crystallization of tristearin differently with respect to kinetics, microstructure as well as phase behavior. Since all these factors are strongly related to the mechanical and thus sensory properties of the fat blends, it is possible to manipulate the structure of the solid fats by incorporating different types of oils which may change the physical properties of the hardstock fats.

3.6 References

1. Awad, T.S., M.A. Rogers, and A.G. Marangoni, *Scaling Behavior of the Elastic Modulus in Colloidal Networks of Fat Crystals.* The Journal of Physical Chemistry B, 2003. **108**(1): p. 171-179.
2. Marangoni, A.G., *The nature of fractality in fat crystal networks.* Trends in Food Science and Technology, 2002. **13**(2): p. 37-47.
3. Narine, S.S. and A.G. Marangoni, *Relating structure of fat crystal networks to mechanical properties: a review.* Food Research International, 1999. **32**(4): p. 227-248.
4. Wright, A.J., et al., *Solvent effects on the crystallization behavior of milk fat fractions.* Journal of Agricultural and Food Chemistry, 2000. **48**(4): p. 1033-1040.
5. Juriaanse, A.C. and I. Heertje, *Microstructure of shortenings, margarine and butter: a review.* Food microstructure., 1988. **7**(2): p. 181-188.
6. Heertje, I., *Microstructural studies in fat research.* Food Structure, 1993. **12**(1): p. 77-94.
7. Wright, A.J., H.D. Batte, and A.G. Marangoni, *Effects of Canola Oil Dilution on Anhydrous Milk Fat Crystallization and Fractionation Behavior.* Journal of Dairy Science, 2005. **88**(6): p. 1955-1965.
8. Ronald M. Krauss, M., Chair; Richard J. Deckelbaum, MD; Nancy Ernst, RD; Edward Fisher, MD; Barbara V. Howard, PhD; Robert H. Knopp, MD; Theodore Kotchen, MD; Alice H. Lichtenstein, DSc; Henry C. McGill, MD; Thomas A. Pearson, MD, PhD; T. Elaine Prewitt, DPH; Neil J. Stone, MD; Linda Van Horn, PhD, RD; Richard Weinberg, MD, Members, *Dietary guidelines for healthy American adults: a statement for health professionals from the Nutrition Committee, American Heart Association.* circulation, 1996. **94**: p. 1795-1800.
9. Hu, F.B., et al., *Dietary Fat Intake and the Risk of Coronary Heart Disease in Women.* New England Journal of Medicine, 1997. **337**(21): p. 1491-1499.
10. Mensink, R.P. and M.B. Katan, *Effect of a Diet Enriched with Monounsaturated or Polyunsaturated Fatty Acids on Levels of Low-Density and High-Density Lipoprotein Cholesterol in Healthy Women and Men.* New England Journal of Medicine, 1989. **321**(7): p. 436-441.
11. Kasai, M., et al., *Effect of dietary medium- and long-chain triacylglycerols (MLCT) on accumulation of body fat in healthy humans.* Asia Pac J Clin Nutr, 2003. **12**(2): p. 151-60.
12. St-Onge, M.P., et al., *Medium-chain triglycerides increase energy expenditure and decrease adiposity in overweight men.* Obesity Research & Clinical Practice, 2003. **11**(3): p. 395-402.
13. Tsuji, H., et al., *Dietary medium-chain triacylglycerols suppress accumulation of body fat in a double-blind, controlled trial in healthy men and women.* Journal of Nutrition, 2001. **131**(11): p. 2853-9.
14. Ho Lam, R.S. and M.A. Rogers, *Experimental validation of the modified Avrami model for non-isothermal crystallization conditions.* CrystEngComm, 2011. **13**(3): p. 866-875.
15. Duval, F., J.M. van Duynhoven, and A. Bot, *Practical implications of the phase-compositional assessment of lipid-based food products by time-domain NMR.* Journal of the American Oil Chemists' Society, 2006. **83**(11): p. 905-912.
16. Mansfield, P., *A new wide-line NMR analyzer and its use in determining the solid-liquid ratio in fat samples.* Journal of the American Oil Chemists' Society, 1971. **48**(1): p. 4-6.
17. Foubert, I., K. Dewettinck, and P.A. Vanrolleghem, *Modelling of the crystallization kinetics of*

fats. Trends in Food Science & Technology, 2003. **14**(3): p. 79-92.

18. Ahmadi, L., A.J. Wright, and A.G. Marangoni, *Chemical and enzymatic interesterification of tristearin/triolein-rich blends: Microstructure and polymorphism.* European Journal of Lipid Science and Technology, 2008. **110**(11): p. 1025-1034.
19. Campos, R., A.G. Marangoni, and M. Ollivon, *Molecular composition dynamics and structure of cocoa butter.* Crystal Growth and Design, 2010. **10**(1): p. 205-217.
20. Chaleepa, K., A. Szepes, and J. Ulrich, *Effect of additives on isothermal crystallization kinetics and physical characteristics of coconut oil.* Chemistry and Physics of Lipids, 2010. **163**(4–5): p. 390-396.
21. Sato, K., *Crystallization behaviour of fats and lipids — a review.* Chemical Engineering Science, 2001. **56**(7): p. 2255-2265.
22. Marangoni, A.G. and S.E. McGauley, *Relationship between crystallization behavior and structure in cocoa butter.* Crystal Growth and Design, 2003. **3**(1): p. 95-108.
23. Alejandro, G.M., *Crystallization Kinetics*, in *Fat Crystal Networks*. 2004, CRC Press. p. 21-82.
24. Long, Y., R.A. Shanks, and Z.H. Stachurski, *Kinetics of polymer crystallisation.* Progress in Polymer Science, 1995. **20**(4): p. 651-701.
25. Alejandro, G.M. and S.N. Suresh, *Microstructure*, in *Fat Crystal Networks*. 2004, CRC Press. p. 179-254.
26. Tang, D. and A. Marangoni, *Microstructure and fractal analysis of fat crystal networks.* Journal of the American Oil Chemists' Society, 2006. **83**(5): p. 377-388.
27. Tang, D. and A.G. Marangoni, *Computer Simulation of Fractal Dimensions of Fat Crystal Networks.* Journal of the American Oil Chemists' Society (JAOCS), 2006. **83**(4): p. 309-314.
28. Shih, W.-H., et al., *Scaling behavior of the elastic properties of colloidal gels.* Physical Review A, 1990. **42**(8): p. 4772-4779.
29. Vreeker, R., et al., *The fractal nature of fat crystal networks.* Colloids and Surfaces, 1992. **65**(2–3): p. 185-189.
30. PORTER, J.D., *The Solubility of Nonelectrolytes. 3rd ed. Joel H. Hildebrand and Robert L. Scott. New York: Reinhold, 1950. 488 pp. $10.00.* Science, 1951. **113**(2938): p. 450-451.

l

4 Micro-Viscosity of Liquid Oil Confined in Colloidal Fat Crystal Networks

H. Du[a], C. Kim[a], M.G. Corradini[a], R.D. Ludescher[a], and M.A. Rogers[a]

**This chapter is published in Soft Matter, *Soft Matter*, 2014,10, 8652-8658 (DOI: 10.1039/C4SM01632G)
Published: Dec, 2014.

4.1 Abstract

Molecular rotors may be utilized as non-invasive, non-disruptive and highly sensitive alternatives to conventional measures of bulk viscosity when the oil is entrained in a colloidal fat crystal network. Oil viscosity changes based on the molecular confinement of the oil, which is dependent on its molecular volume. Changes in micro-viscosity were not dependent on the solids content, but instead were strongly dependent on the box-counting fractal dimension in high-space filling colloidal fat crystal networks (i.e., $D > 1.89$). A bulk oil viscosity is often an overestimation of the actual viscosity of the entrained oil and may not be appropriate when predicting diffusion in multi-phase materials.

4.2 Introduction

Gels comprised of self-associating colloidal networks have unique applications as elastic biomaterials in foods,[1-3] medicine,[4] inks,[5] and pharmaceutical delivery agents.[6] The capacity of the network to entrap the continuous liquid phase directly influences stability, permeability and functionality.[7] This is of utmost importance in edible colloidal fat crystal networks, where the ability of the network to entrain the liquid component directly influences oil mobility.[7] For example, mobility of oil in chocolate-based products accelerates bloom and softening.[8-11] Although the macroscopic measurement of oil mobility in colloidal networks is relatively straightforward,[7, 12] the influence of the colloidal nature of the network on the

confinement and hence viscosity of oil is not well understood.

Numerous mechanisms have been proposed for the driving force for oil migration, which arises based on either differences in liquid fat content or a gradient in triacylglycerol concentration.[12, 13] Using an unsteady state concentration gradient of one component as the driving force for diffusion, Fick's second law may be extended to:[13]

$$\frac{\partial c}{\partial t} = \frac{\partial}{\partial x}\left(D\frac{\partial c}{\partial x}\right) \quad (1)$$

where c is the concentration, t is time, x is the distance and D is the diffusivity. The diffusivity takes the following form:

$$D = -\frac{kT}{6\pi\eta r} \quad (2)$$

where k is Boltzman constant, T is the absolute temperature, η is the viscosity and r is the molecular radius of the diffusing particle. Irrespective of the underlying driving force and theory used to describe the mobility, in colloidal networks, a permeability coefficient, β, and viscosity, η, are often combined in the form of Darcy's Law:

$$Q = \frac{\beta A_c}{\eta} \times \frac{\Delta P}{L} \quad (3)$$

where Q is the volumetric flow rate, A_c is the cross sectional area, η is the viscosity of the liquid oil, and ΔP is the pressure drop over the distance, L. β is dependent on numerous structural characteristics including particle radius, a, a tortuosity factor, K, the solids content, ϕ, and the fractal dimension, D_f.[14]

$$\beta = \left(\frac{a^2}{K}\right)\phi^{2/(D_f-3)} \quad (4)$$

In general, the microstructural elements of colloidal fat crystal networks such as the particle size, tortuosity and fractal dimension may be accessed using simple techniques including: microscopy, rheology and/or light scattering techniques. However, the viscosity is not a measure of the macroscopic viscosity of the material but instead of the viscosity of the entrained liquid oil, as this is the path of migration.[13] It is the objective of this manuscript to determine if the confinement of liquid oil in a colloidal fat crystal network alters the viscosity of the continuous phase using molecular rotors. The use of fluorescent molecular rotors can, in principle, enable the sensitive characterization of the microenvironment in fat crystal networks.

Molecular rotors define molecules that consist of two or more parts that can easily rotate relative to each other.[15, 16] Upon photoexcitation these compounds can undergo twisted intra-molecular charge transfer (TICT) which is the rotation of one of the segments of the molecule relative to the other.[17] Deactivation from the TICT state occurs through a nonradiative pathway, and radiative decay, which results in emission of a photon, is observed from the locally excited state. These two competing relaxation pathways determine the sensitivity of the probe to the micro-viscosity of the surrounding environment since TICT state formation rate is lower in more viscous environments.[18-20] In a less viscous fluid environment the molecule undergoes fast internal rotation (Figure 1), and thus fast radiationless

decay.[21] Environmental restrictions to intramolecular twisting result in an increase in fluorescence emission. Changes in emission properties of fluorescent molecular rotors (specifically, fluorescence quantum yield, intensity and lifetime) have been correlated to the local (or micro) and bulk viscosity of the medium,[22] polymerization and aggregation processes,[17] and phase transitions.[18]

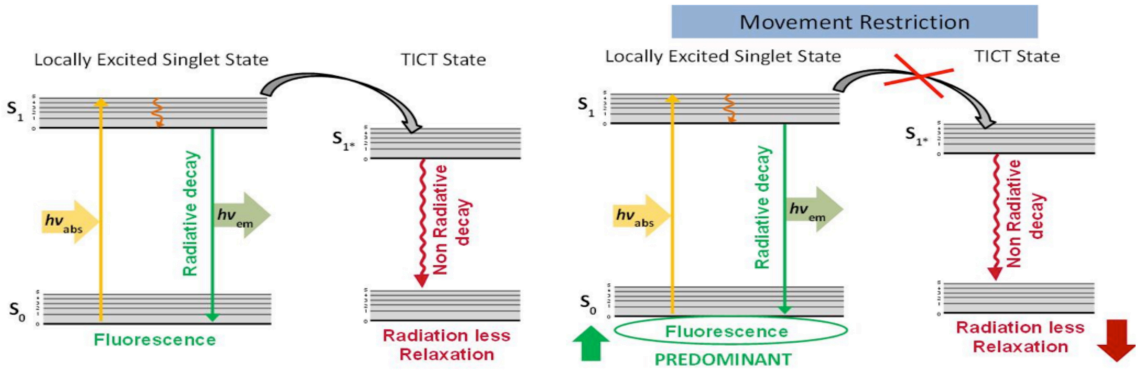

Figure 1. Jablonski diagram of a single emission band molecular rotor. Left- Notice that relaxation from the TICT state occurs without fluorescence emission. Right - Restriction of the twisted state increases fluorescence emission. Adapted from Haidekker and Theodorakis.[18]

4.3 Methods

Tristearin was used as the solid component and the liquid oil was either a medium-chain triglyceride oil (i.e., tricaproin, tricaprylin, and tricaprin) or an unsaturated oil (i.e., triolein and trilinolein) (Sigma Aldrich, St. Louis, MO, USA). Fat blends were prepared from 30 to 100 wt% tristearin at 10 wt% intervals in each liquid oil. The blends were heated to 80 ^{o}C, above the melting point of tristearin, and held for 20 min and then stored for 24 hrs in a 35 ^{o}C temperature controlled incubator

before analysis.

4.3.1 Solid fat content

Samples were subjected to T_2 relaxation measurements on a Bruker mq20 Series NMR Analyzer (Bruker, Milton, Ontario, Canada). A Hahn-echo pulse sequence was used to measure the free induction decay (FID), T_2 relaxation of the solid crystalline component (< 70 μs) of the blends.[23, 24] The operational pulse length was obtained using the calibration procedures recommended by the manufacturer. The 90^o pulse was 2.6 μs and the 180^o pulse was 5.1 μs. This allowed determination of the gain (64) and recycle delay (5 sec). Tau was selected to be as short as possible (0.5 ms) to minimize chemical exchange and diffusion effects on the decay curves.

4.3.2 Polarized light microscopy and fractal analysis

The supramolecular structure of the fat blends were imaged using a Linkham Imagining Station (Linkham, Surrey, England) equipped with a Q imagining 2560 x 1920 pixel CCD camera (Micropublisher, Surrey, Canada) and a 10 X Olympus lens (0.25 N.A.) (Olympus, Tokyo, Japan). Samples were placed on a glass slide and a cover slip was set on top of the sample. The slide was transferred into a Peltier temperature control stage (LTS120, Linkham, Surrey, England) using a water reservoir as the heat sink and imaged at 35 ^oC to observe crystal structure using non-polarized light. Light micrographs were calibrated with a 100 μm micrometer.

Using the polarized light micrographs, Image J (NIH, Bethesda, MD) was used to calculate a box-counting fractal dimension, D_f, using the fractal dimension and lacunarity, FracLac, plugin.[25] The box-counting algorithm is a simple method to quantify complex structures by laying successively sized grids over digital images and the foreground pixels (the crystal area) are counted in each box. Boxes must be completely void of crystals to be excluded. D_f is calculated using the relationship between the number of boxes containing crystals, N, and the size of the overlaying box, ε:

$$N \propto \varepsilon^{-D_f} \tag{5}$$

4.3.3 Micro-viscosity

1-(2,5-dimethoxy-phenylazo)-naphthalen-2-ol (Citrus red 2 (CR)) was purchased from Sigma-Aldrich (St. Louis, MO, USA) and used without further purification. Stock solutions (1mM) of this food dye were prepared in DMSO, ethanol, ethylene-glycol 99% purity, glycerol (spectrophotometric quality – 99.5% purity), hexane and tricaprylin. The stock solutions were used to obtain CR excitation and emission spectra and to assess the viscosity and *polarity* sensitivity of CR's fluorescence intensity in solutions. DMSO, ethanol, hexane and polyols were obtained from Fisher Scientific (Pittsburgh, PA).

4.3.4 Fluorescence emission of Citrus red 2 in polar protic, polar aprotic and nonpolar solvent solutions

Since limited information on the photophysical properties of CR is available, stock solutions of CR were diluted to 10 uM to obtain the fluorescence excitation and emission spectra of the dye in protic, aprotic and nonpolar solvent solutions. Steady state fluorescence excitation and emission spectra were recorded using a Fluoromax-3 spectrofluorometer (Horiba Scientific Inc., Edison, NJ). 10 uM CR solutions were tested in 1 cm lightpath quartz cuvettes (NSG Precision Cells, Farmingdale, NY) at 35 ^{o}C. Preliminary runs were conducted to identify the optimal excitation wavelength and emission and excitation slits for each sample. The fluorescence emission intensity in counts per second, peak emission and excitation wavelength were determined. The effect of dye concentration on fluorescence intensity was further tested in order to minimize inner filter effects in subsequent studies.

4.3.5 Citrus red fluorescence emission in solutions of different viscosities

To assess CR sensitivity to viscosity, the fluorescence emission intensity of 10 uM solutions of CR in binary mixtures of ethylene glycol and glycerol was recorded using a Fluoromax-3. All measurements were performed at 20 ^{o}C. As reported in the literature [19, 26, 27] variations in viscosities within a 15-400 mPa s range can be obtained by modifying the ethylene glycol (low viscosity solvent)-glycerol (high viscosity solvent) ratio. The dependence of CR fluorescence intensity on the surrounding medium's viscosity was also assessed in pure glycerol whose viscosity

was modified using temperature to attain values between 30-12000 mPa s.

The Förster and Hoffman equation relates the fluorescent quantum yield, Φ_F, of a molecular rotor to the viscosity (η) of the surrounding solution.[28] This relationship can be described as follows (Eq. 6):

$$\log \Phi_F = C + x \log \eta \quad (6)$$

where C and x are solvent and dye dependent constants.

Since fluorescence emission intensity, I_F, and quantum yield are proportional, the relationship between fluorescence intensity and viscosity can be reworked from Eq. 5 and expressed by the following power law model (Eq. 7):[18]

$$I_F = \alpha \eta^x \quad (7)$$

where α can be considered a measure of the probe's brightness and x a measure of its sensitivity to local viscosity.[27] The relationship between maximum fluorescence intensity and viscosity of the CR solutions was fitted using Eq. 7 and sensitivity of CR to viscosity (x) was compared to reported values of commonly used molecular rotors in similar systems. The applicability of Eq. 7 was also verified by the linear correspondence of fluorescence intensity and viscosity plotted in a double-logarithmic scale.

4.3.6 Evaluation of microenvironment in confined solid fat networks using Citrus red

Movement restriction of a molecular rotor, in this case CR, results in noticeable increase in fluorescence emission intensity. Based on this observation a spectrofluorometric technique was developed to characterize the microenvironment in solid fat networks. 10 mM CR stock solutions were prepared in five triacylglycerols, namely tricaproin, tricaprylin, tricaprin, triolein and trilinolein, all of which are liquid a room temperature. CR was embedded in the fat blends by partial substitution of the liquid oil solvent by the corresponding CR stock solution to attain a final concentration of the fluorescent dye of 0.85 mM. The concentration in the fat blends was higher than that used in solutions to account for the lack of clarity in the solid fat samples.

Once the fat blends were prepared with and without the addition of CR, they were heated up to completely melt the solid fat component. A 10 uL aliquot of each mixture was deposited on the center of custom-made quartz slides (10 mm x 25 mm, NSG Precision Cells). The slides were kept at 40 ^{o}C to facilitate dispensing of the complete volume and prevent solidification of the fat mixture upon contact with a cold surface. The dimensions of the sample were checked for consistency using a caliper. The samples were incubated at 35 ^{o}C for at least 24 hrs before testing. The slides were inserted at a 45^{o} angle in a 1 cm light-path quartz cuvette. Their fluorescence emission spectra were recorded using a Fluoromax-3. On the emission

end a 550 nm longpass cut-on filter was mounted to eliminate disturbances by scattered excitation light. The excitation wavelength and the excitation and emission slits were set at 540 nm and 3 nm, respectively. The fluorescence emission spectra were normalized and the blank subtracted from the corresponding CR spectra. All samples were run at least in triplicate.

4.4 Results and Discussion

Synthetic food colors are widespread in products due to their stability and functionality at low concentrations. 1-(2,5-dimethoxy-phenylazo)-naphthalen-2-ol (Citrus red 2 - CR) is a color additive normally applied to the surface of fresh oranges to enhance their external appearance. CR was selected based on its solubility (insoluble in water, soluble in organic solvents) and ready availability. Additionally, preliminary results indicated easy differentiation of the emission band of CR from background noise.

As seen in Fig. 2, Citrus red 2 contains one functional azo group. The presence of the azo group potentially confers molecular rotor properties to this dye such that it exhibits low fluorescence emission intensity in low viscosity fluid solutions and a significant enhancement of fluorescence intensity in highly viscous solvents. Abbott et al. [29] have studied the dynamics of excited states of azo dyes in solutions. Their estimations indicate that excited state tautomerization and/or internal twisting are likely to constitute the predominant nonradiative relaxation pathway in azo dyes in

low viscosity solutions.

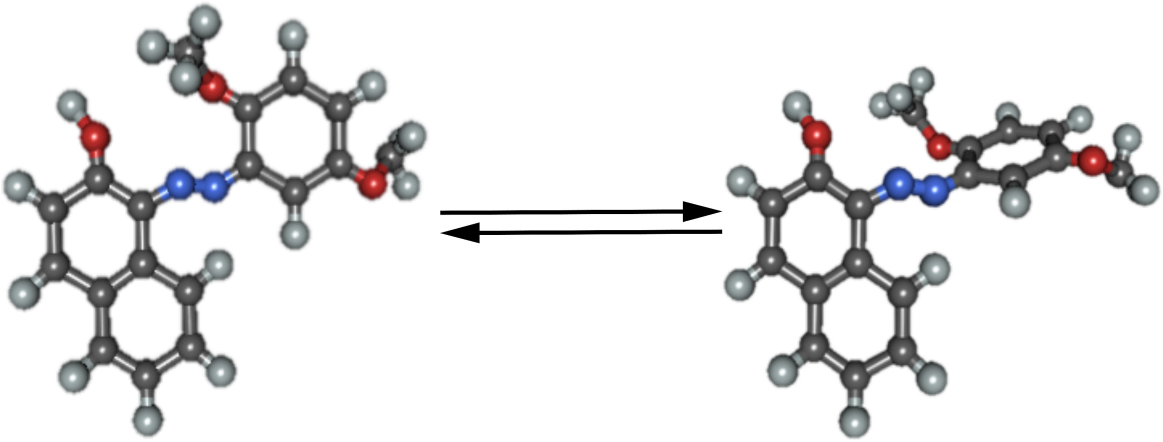

Figure 2. Structure and possible intramolecular rotation in Citrus Red 2.

Emission and excitation spectra of CR in polar protic (ethanol, ethylene glycol and glycerol) solutions and emission spectra as a function of polarity are shown in Fig. 3 A and B, respectively. The data were normalized towards CR in glycerol to illustrate the effect of the surrounding viscosity on the fluorescence intensity of CR. As can be observed in Fig 3, CR is practically non emissive in common solvents, which can explain the limited information on its photophysical properties.

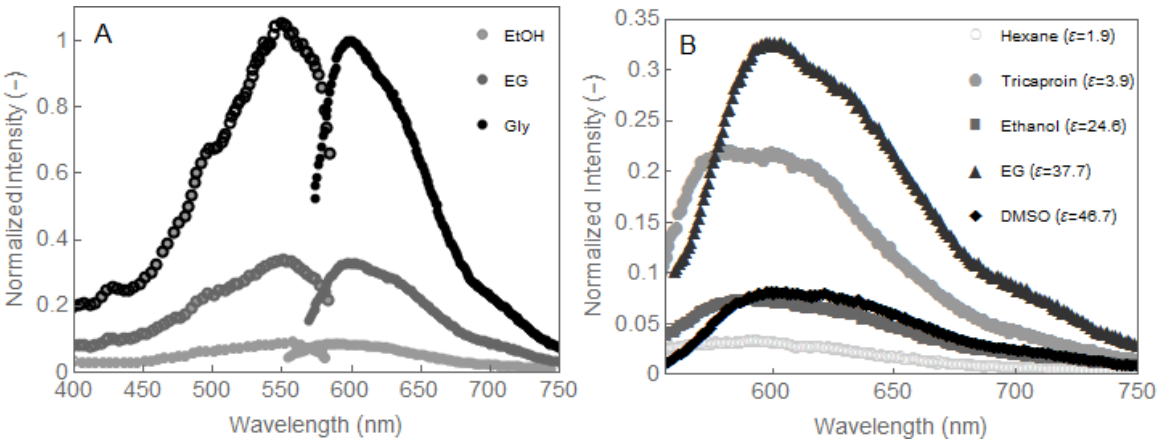

Figure 3. A- Excitation (empty circles) and emission (solid circles) spectra of CR in

solvents of similar polarity and different viscosity. B- Effect of polarity on the emission spectra of CR. Permittivity (ε) of solvents is reported between brackets.

CR's Stokes shift, (ℓ_{em}-ℓ_{exc}), was estimated to be 45-60 nm depending on the medium. Environmental polarity only moderately impacted the location of the peaks and, consequently, Stokes shift. Although a bathochromic shift was observed as the polarity of the solvents increased, the magnitude of the shift (~15 nm) was equivalent to that of other commonly reported molecular rotors in similar environments, for example, 9-(2,2-dicyanovinyl)-julolidine (DCVJ).[30]

The sensitivity of CR fluorescence emission intensity to the medium's rigidity, evaluated as viscosity of the surrounding media, is shown in Figs. 4 and 5. To facilitate comparison within each experiment, the data were normalized so that the emission from the highest viscosity corresponds to unity. The maximum fluorescence intensity of CR increases as the viscosity of the surrounding media increases, regardless if the change in viscosity was temperature or concentration driven. Although the data were plotted in double logarithmic coordinates to verify the applicability of Eq. 7, the parameters of the power law relationship were obtained using a nonlinear regression procedure to minimize bias in the estimation.[31]

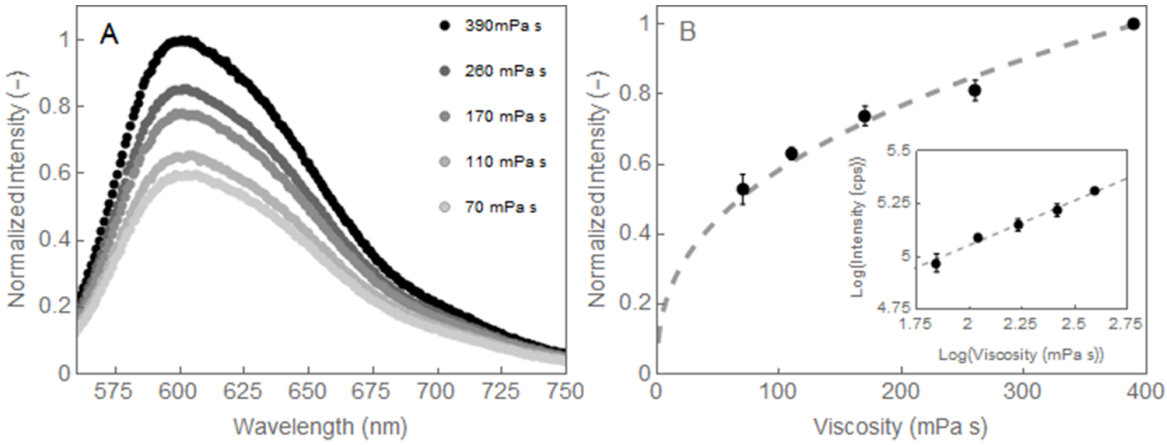

Figure 4. (A) Emission spectra of CR in ethylene glycol and glycerol mixtures. (B) Dependence of CR fluorescence intensity on viscosity fitted with Eq. 7. Inset: Relationship presented as a log-log plot.

While the maximum theoretical viscosity sensitivity of molecular rotors has been estimated to be 0.66, sensitivity values (x) of novel and commonly used molecular rotors have been reported in the range of 0.25 to 0.6 (i.e., 0.26-0.4 for modified nucleosides,[32] 0.53 for DCVJ, 0.52 for 9-(2-carboxy-2-cyano)vinyl julolidine (CCVJ)[30] and 2-cyano-3-(4-dimethylaminophenyl) acrylic acid methyl ester (CMAM).[33] In the case of CR, the viscosity sensitivity was established to be 0.43, within the range reported for other molecular rotors.

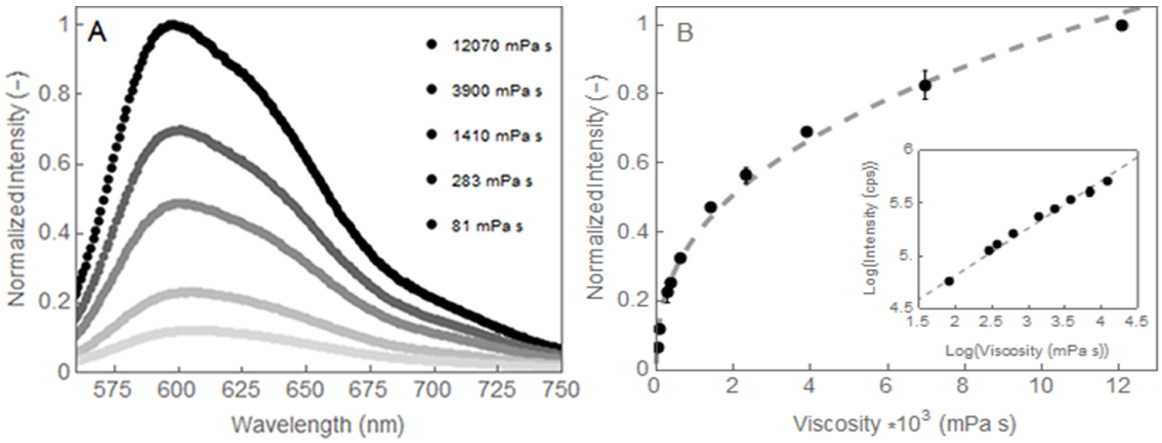

Figure 5. (A) Emission spectra of CR in glycerol at different temperatures. (B)

Dependence of CR fluorescence intensity on viscosity fitted with Eq. 7. Inset: Relationship presented as a log-log plot.

A large Stokes shift and high sensitive to viscosity (or molecular rigidity) changes are two requirements of an adequate molecular rotor.[27] In principle, the behaviour of CR in relation to these two conditions, which is comparable that of other commonly used or recently proposed molecular rotors, establishes CR's molecular rotor character and supports its potential use as a probe of micro-viscosity or molecular crowding in solid fat networks. It should be also noticed that when CR was incorporated in solid fat samples, in contrast to reference samples stained with DCVJ, the location of its emission peak at about 600 nm and its Stokes shift facilitated differentiation from background noise. Examples of the emission spectra of CR in a solid fat crystal network of a saturated medium chain TAG (A) or an unsaturated long chain TAG (B) and tristearin are presented in Fig. 6. The shown emission spectra were obtained by subtracting the background spectra of each respective dye-free controls and correcting for scattering and dye concentration.

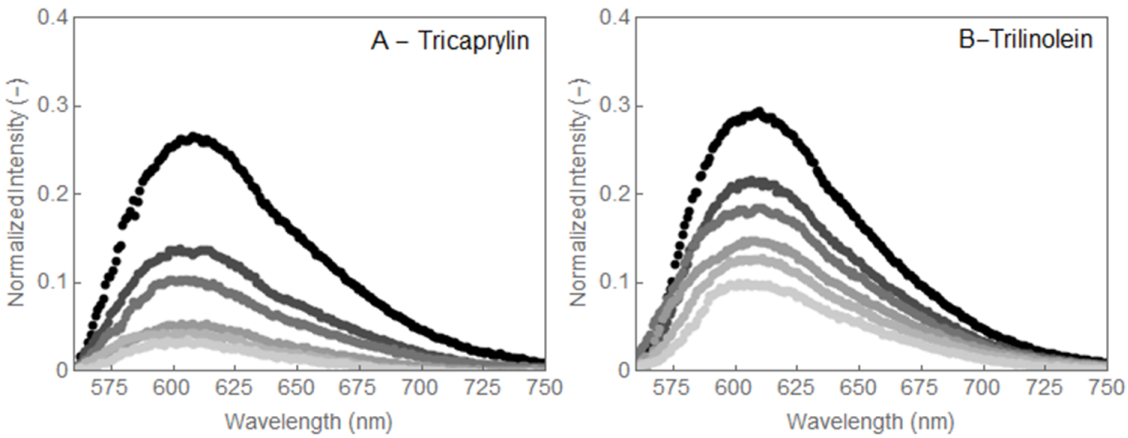

Figure 6. Normalized fluorescence emission spectra of CR in saturated medium chain TAG and tristearin (A) and unsaturated long chain TAG and tristearin (B) solid fat crystal networks. Black: highest proportion of solid fat. Lightest gray: lowest solid fat proportion.

Using the normalized intensities of the emission spectra, which are relative to the viscosity in the microenvironment, it is observed that the viscosity decreases as the solid tristearin content decreases (Figure 7). However, there are no obvious trends that correlate these two parameters. It is not surprising that the confinement of liquid oil is not simply proportional to the solids; numerous other microstructural elements including crystal size, crystal number, distribution, etc. affect the interactions between the continuous oil and solid crystal phases.

In an attempt to better characterize the microstructural elements, polarized light micrographs were obtained for each of the different fat blends (Figure 8). Visually, no obvious differences are observed between blends nor the type of liquid oil. Since no clear trend was initially obvious, microstructural differences were systemically characterized using box-counting fractal dimensions that have been extremely well documented for fat crystal networks.[34, 35] A box-counting fractal dimension, D, is calculated by superimposing grids with side length, l, over a threshold binary image of a fat crystal network with the grids containing particles more than a threshold value being defined as the occupied grids.[36] Early work by Litwinenko et al., has shown that the box-counting fractal dimension is highly sensitive to the space filling

colloidal network.[37]

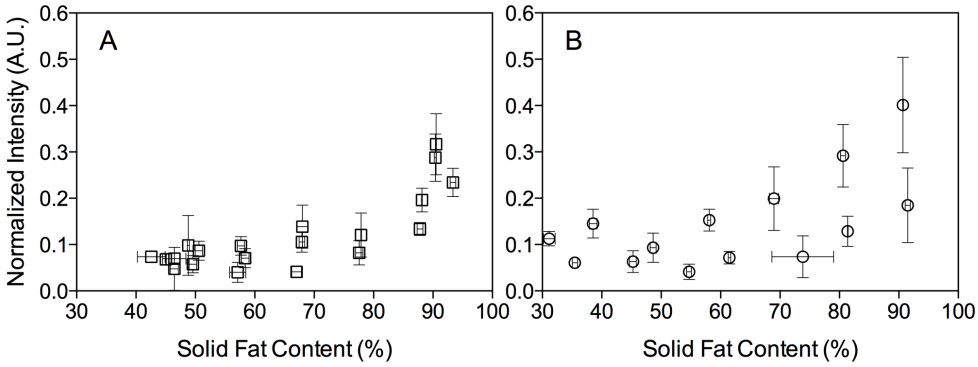

Figure 7. Normalized intensity of CR in each blended fat as a function of the solid fat content in medium chain triglycerides (tricaproin, tricaprylin, and tricaprin) (A) and unsaturated triglycerides (triolein and trilinolein) (B).

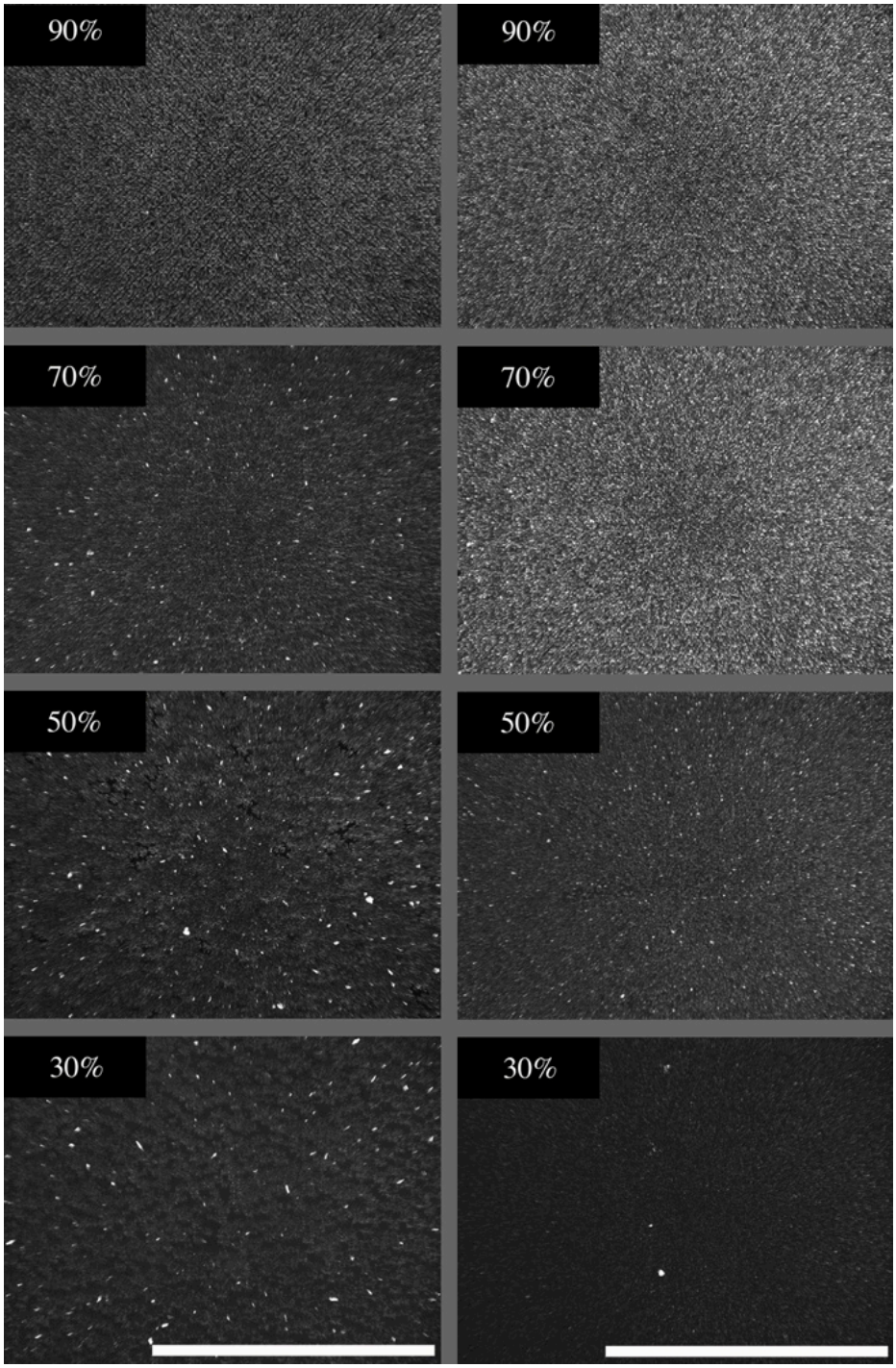

Figure 8: Polarized light micrographs of tristearin blends with different % solids fat contents of tricaprin (left) and triolein (right). The scale bar = 100 μm.

Over small changes in solid fat content there is often a linear correlation with the fractal dimension, however it has been shown that non-linear relationships exist when the solid fat content varies greatly (Figure 9).[38, 39] For medium chain triglycerides,

there is a linear relationship with the fractal dimension until approximately 60 % SFC, after which there is a precipitous drop in fractal values (Figure 9A). Also, non-linear relationships between the SFC and fractal dimensions exist for the unsaturated triglycerides (Figure B). Due to the non-linear relationship between these variables, it was believed that the viscosity might perform better as a function of the box-counting fractal dimension.

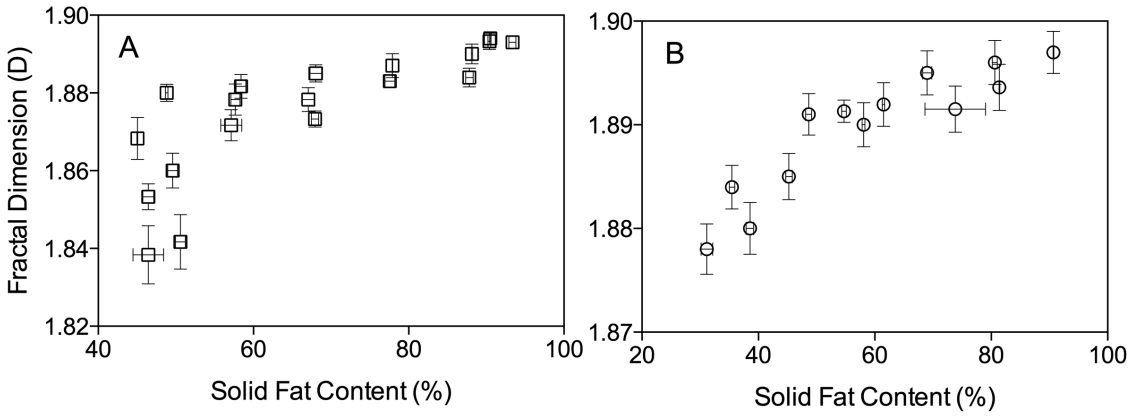

Figure 9: Box-counting fractal dimension in medium chain triglycerides (tricaproin, tricaprylin, and tricaprin) (A) and unsaturated triglycerides (triolein and trilinolein) (B) as a function of solid fat content.

Using the box-counting fractal dimension, a strong log-logistic correlation with the normalized intensity of CR (Y) in the blended fats was observed (Figure 10).

$$Y(x) = a + log\left(1 + e^{(k*(x-c))}\right) \qquad (8)$$

where a is the baseline intensity (i.e., viscosity of liquid oil), k is the rate of change of the normalized intensity as a function of the fractal dimension, and c

is the critical fractal dimension at which a pronounced change in intensity is observed. Using the parameters obtained from the fits (Table 1), numerous very important insights on the confinement of liquid oil in colloidal fat crystal networks are obtained.

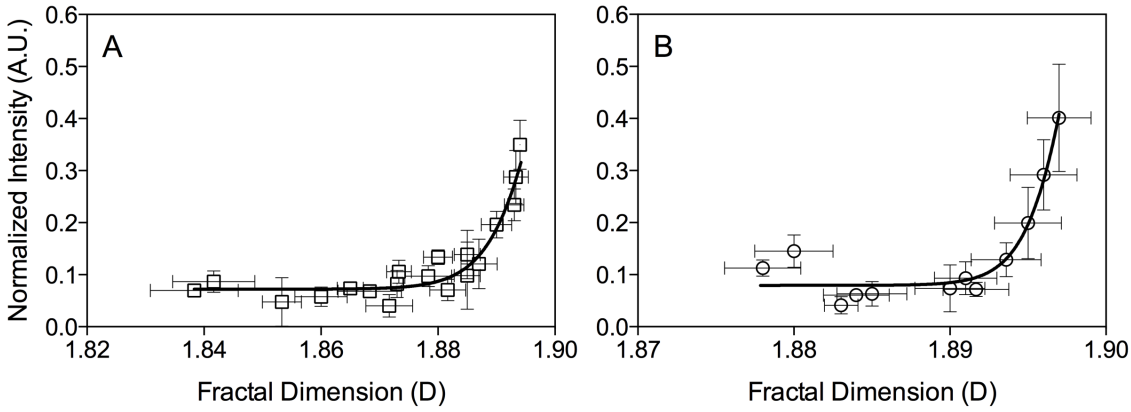

Figure 10: Normalized intensity of CR in each blended fat as a function of the box-counting fractal dimension in medium chain triglycerides (tricaproin, tricaprylin, and tricaprin) (A) and unsaturated triglycerides (triolein and trilinolein) (B).

Table 1: Fitted parameters to the log-logistic fit between the normalized intensity and fractal dimension.

	a	k	c	R^2
Medium Chain TAGs	$7.22 \times 10^{-2} \pm 0.71 \times 10^{-2}$	265.3 ± 33	1.896±0.0005	0.81
Unsaturated TAGs	$7.95 \times 10^{-2} \pm 1.00 \times 10^{-2}$	609.7 ± 99	1.897±0.0001	0.82

Of the fitted parameters, the slope, k, and the critical fractal dimension, c, provide two very important insights into understanding liquid oil confinement in colloidal fat crystal networks. Since the data set is normalized, the baseline intensity does not provide significant insights. When the fractal dimension was below 1.89,

irrespective of the solvent used, the confinement did not alter the micro-viscosity of the oil. Therefore, when studying oil migration, the effect of confinement may not be significant in low fractal dimension fat blends. However, when the fractal dimension is above 1.89, which is very common, using the viscosity of the bulk liquid oil is likely not representative of the system and as such the micro-viscosity may be an attractive method.

The rate constant, k, for the normalized intensity versus the fractal dimension is much steeper for unsaturated oil (18:1 and 18:2) compared to the medium chain triglycerides (6:0, 8:0 and 10:0). When comparing the k parameters for the unsaturated oil and medium chain triglycerides it is observed that the viscosity as a function of the box-counting fractal dimension increased at a ratio of 2.3:1. As the box-counting fractal dimension increases, the space-filling network also increases which would result in a decrease in the void volume where the liquid oil is confined. It is hypothesised that as the inter-crystal space decreases there will be a greater increase in viscosity for oils with lower molecular volumes. The molecular volumes were predicted using ACD percepta (ACD Inc., Toronto, ON). The average molecular volume for the medium chain triglycerides was 485 cm^3/mol (tricaproin (386 cm^3/mol), tricaprylin (485 cm^3/mol), and tricaprin (584 cm^3/mol)) and for the unsaturated oils 951 cm^3/mol (triolein (961 cm^3/mol) and trilinolein (941 cm^3/mol)). The ratio of the molecular volumes for the unsaturated oils and medium chain triglycerides was 2.3:1, corresponding remarkably well to the ratio of the rate

constants. This fluorescence correlation suggests that the oil viscosity at fractal dimension greater than 1.89 will change more for long-chain unsaturated oils compared to the medium chain triglycerides. The sensitivity of a molecular rotor to changes in viscosity is based on steric hindrance of intramolecular rotation, which is related to molecular free volume and molecular crowding around the probe,[18, 32] hence the correlation between fractal dimension and fluorescence intensity.

4.5 Conclusions

The use of molecular rotors offers a non-invasive, non-disruptive and highly sensitive alternative to conventional analytical methodologies to evaluate the microenvironment in a fat crystal network. It is clear that the molecular confinement of the oil is dependent on its molecular volume and is strongly dependent on the microstructural elements including the box-counting fractal dimension in high-space filling colloidal fat crystal networks (i.e., $D > 1.89$). Simply using a bulk oil viscosity may not be appropriate in predicting diffusion of multi-phase materials containing oils as the continuous phase.

4.6 Acknowledgements

This project was supported by the Agriculture and Food Research Initiative Grant no. 2014-67017-21649 from the USDA National Institute of Food and Agriculture, Improving Food Quality –A1361 as well as a seed grant from the New Jersey Institute

of Food, Nutrition & Health.

4.7 References

1. Norton, J.E. and I.T. Norton, *Designer colloids—towards healthy everyday foods?* Soft Matter, 2010. **6**: p. 3735-3742.
2. Marangoni, A.G., et al., *Structure and functionality of edible fats.* Soft Matter, 2012. **8**: p. 1275-1300.
3. Dickinson, E., *Stabilising emulsion-based colloidal structures with mixed food ingredients.* Journal of the Science of Food and Agriculture, 2013. **93**: p. 710-721.
4. Farhari, A., Q. Phan, and C. Berkland, *Hyaluronic acid colloidal gels as self-assembling elastic biomaterials.* Journal of Biomedical Materials Research Part B, 2014. **102**: p. 612-618.
5. Ko, H.-Y., et al., *Rapid Self-Assembly of Monodisperse Colloidal Spheres in an Ink-Jet Printed Droplet.* Chemistry of Materials, 2004. **16**: p. 4212-4215.
6. Vinogradov, S.V. and A.V. Kabanov, *Nanogels as Pharmaceutical Carriers: Finite Networks of Infinite Capabilities.* Angewandte Chemie International Edition, 2009. **30**: p. 5418-5429.
7. Dibildox-Alvarado, E., et al., *Effects of Crystalline Microstructure on Oil Migration in a Semisolid Fat Matrix.* Crystal Growth & Design, 2004. **4**: p. 731-736.
8. Bricknell, J. and R.W. Hartel, *Relation of fat bloom in chocolate to polymorphic transition of cocoa butter.* Journal of the American Oil Chemists' Society, 1998. **75**: p. 1609-1615.
9. Campos, R. and A.G. Marangoni, *Crystallization Dynamics of Shear Worked Cocoa Butter.* Crystal Growth & Design, 2014. **14**: p. 1199-1210.
10. Maleky, F., et al., *Effect of Cocoa Butter Structure on Oil Migration.* Journal of Food Science, 2012. **77**: p. E74-E79.
11. Galdamez, J.R., et al., *Oil migration in chocolate: A case of non-Fickian diffusion.* Journal of Food Engineering, 2009. **92**: p. 261-268.
12. Timms, R.E., *Confectionery Fats Handbook*. 2003, Bridgwater, England, U.K. : The Oily Press.
13. Ghosh, V., G.R. Ziegler, and R.C. Anantheswaran, *Fat, moisture, and ethanol migration through chocolate and confectionery coatings.* Critical Reviews in Food Science and Nutrition, 2002. **42**: p. 583–626.
14. Bremer, L.G.B., T. vanVliet, and P. Walstra, *Theoretical and experimental study of the fractal nature of the structure of casein gels. .* Journal fo the Chemical Society: Faraday Transactions, 1989. **85**: p. 3359-3372.
15. Ichimura, K., et al., *Photo‐optical liquid crystal cells driven by molecular rotors.* Applied Physical Letters, 1993. **63**: p. 449-451.
16. Kottas, G.S., et al., *Artificial molecular rotors.* Chemical Reviews, 2005. **105**: p. 1281-1376.
17. Uzhinov, B.M., V.L. Ivanov, and M. Ya Melnikov, *Molecular rotors as luminescence sensors of local viscosity and viscous flow in solutions and organized systems.* Russian Chemical Reviews, 2011. **80**: p. 1179 – 1190.
18. Haidekker, M.A. and E.A. Theodorakis, *Environment-sensitive behavior of fluorescent molecular rotors. .* Journal of Biological Engineering, 2010. **4**: p. 1-14.
19. Loutfy, R.O. and B.A. Arnold, *Effect of viscosity and temperature on torsional relaxation of molecular rotors.* The Journal of Physical Chemistry, 1982(86): p. 4205-4211.
20. Law, K.Y., *Fluorescence probe for microenvironments: anomalous viscosity dependence of the fluorescence quantum yield of p-N,N-dialkyl-amino-benzylidene-malononitrile in 1-alkanols. .* Chemical Physics Letters, 1980. **75**: p. 545–549.

21. Lakowicz, J.R., *Principles of Fluorescence Spectroscopy. 3rd Ed.* 2006, Baltimore, MD, USA: Springer Science + Business Media.
22. Turro, N.J., V. Ramamurthy, and J.C. Scaiano, *Modern molecular photochemistry of organic molecules*. 2010, Herndon, VA, USA. : University Science Books.
23. Mansfield, P.B., *A new wide-line NMR analyzer and its use in determining the solid-liquid ratio in fat samples.* Journal of the American Oil Chemists Society, 1971. **48**: p. 4-6.
24. Duval, F.P., J.P.M. van Duynhoven, and A. Bot, *Practical implications of the phasecompositional assessment of lipid-based food products by time-domain NMR.* Journal of the American Oil Chemists Society, 2006. **83**: p. 905-912.
25. Karperien, A. *User's Guide for FracLac*. 2007 [cited 2014 July, 8, 2014]; Available from: http://imagej.nih.gov/ij/plugins/fraclac/FLHelp/Introduction.htm - menu2.
26. Lang, J.M., Z.A. Dreger, and H.G. Drickamer, *A high pressure study of the effect of viscosity on the light induced isomerization of DMABN in three linear alcohols, iso-butanol and glycerol.* Chemical Physics Letters, 1995(243): p. 78-84.
27. Sutharsan, J., et al., *Molecular rotors: synthesis and evaluation as viscosity sensors.* Tetrahedron, 2010. **66**: p. 2582–2588.
28. Förster, T. and G. Hoffmann, *Die Viskositätsabhängigkeit der Fluoreszenzquantenausbeuten einiger Farbstoffsysteme.* Zeitschrift für Physikalische Chemie Neue Folge, 1971. **75**: p. 63–76.
29. Abbott, L.C., et al., *Picosecond deactivation of azo dye excited states in solution and in cellulose.* Journal of Photochemistry and Photobiology A: Chemistry, 2011. **218**: p. 11–16.
30. Haidekker, M.A., et al., *Effects of solvent polarity and solvent viscosity on the fluorescent properties of molecular rotors and related probes.* Bioorganic Chemistry, 2005. **33**: p. 415–425.
31. Van Boekel, M.A.J.S., *Kinetic Modeling of Food Quality: A Critical Review.* Comprehensive Reviews in Food Science and Food Safety, 2008. **7**: p. 144-158.
32. Sinkeldam, R.W., et al., *Emissive Nucleosides as Molecular Rotors.* ChemPhysChem, 2011. **12**: p. 567–570.
33. Yasuhara, K., Y. Sasaki, and J. Kikuchi, *Fluorescent sensor responsive to local viscosity and its application to the imaging of liquid-ordered domain in lipid membranes.* Colloids and Surfaces B: Biointerfaces,, 2008. **67**: p. 145–149.
34. Tang, D. and A.G. Marangoni, *Microstructure and Fractal Analysis of Fat Crystal Networks.* Journal of the American Oil Chemical Society, 2006. **83**: p. 377-388.
35. Tang, D. and A.G. Marangoni, *Computer Simulation of Fractal Dimensions of Fat Crystal Networks.* Journal of the American Oil Chemical Society, 2006. **83**: p. 309-314.
36. Tang, D. and A.G. Marangoni, *Quantitative study on the microstructure of colloidal fat crystal networks and fractal dimensions.* Advances in Colloid and Interface Science, 2006. **128-130**: p. 257-265.
37. Litwinenko, J.W., et al., *Relationship between crystallization behavior, microstructure and mechanical properties in a palm-oil based shortening.* Journal of the American Oil Chemists Society, 2002. **79**: p. 647-654.
38. Awad, T.S., M.A. Rogers, and A.G. Marangoni, *Scaling behavior of the elastic modulus in colloidal networks of fat crystals.* Journal of Physical Chemistry B, 2004. **108**(1): p. 171-179.
39. Marangoni, A.G. and M.A. Rogers, *Structural basis for the yield stress in plastic disperse systems.* Applied Physics Letters, 2003. **82**(19): p. 3239-3241.

5 Conclusions

The work from this thesis first investigated the effect of different liquid oils on the crystallization of solid fat and the results revealed that the interaction between solid fat and liquid oil in a blended system can be very different depending on the structure of the oil triglycerides. The MCTs change the nucleation mode of crystallization of tristearin from instantaneous to sporadic while the unsaturated triglycerides do not have this influence. The microstructure of the tristearin crystal network is also affected differently by MCTs and unsaturated triglycerides which could be due to a different crystal packing manner, crystal size or crystal distribution. According to the phase behavior results, it is suggested that MCTs oils can co-crystalize with tristearin and thus could strengthen the crystal network rather than simply diluting the solid fat crystals. Due to the time frame limitations, the types and the numbers of the liquid oil we study was also limited but still it provides evidence that it is possible to manipulate the physical properties of the hardstock fats by incorporating different types of the liquid oils which could be easier and more sensory acceptable than looking for a totally non-fat fat replacer to achieve mechanical property wanted as well as keep the nutrition value.

The second part of the thesis examined the liquid oils confined in a tristearin crystal network. In order to measure the viscosity under this confinement effect, molecular rotors were used. Citrus red 2 which is a GRAS food colorant was sensitive enough to measure the micro viscosity. The viscosity measurement of six different

oils showed that the molecular confinement of the oil was strongly dependent on the box-counting fractal dimension in high-space filling colloidal fat crystal networks rather than simply the solid fat content. Therefore, this confinement effect should be taken into consideration when predicting diffusion of oils in multi-phase materials with oil continuous phase instead of simply using a bulk oil viscosity.